N° d'ordre :

N° de série :

People's Democratic Republic of Algeria

Ministry Of Higher Education And Scientific Research

University Of Ghardaia Faculty of Science and Technology

Department of Automatics and Electromechanics

A thesis submitted in fulfillment of the requirements for the degree of MASTER

Domain : Sciences and Technologies

Branch : Automatics

Specialty : Automatics and systems

Theme

Smart Drone Technology for Comprehensive Wheat Silo Inspection: Integrating Normal and Thermal Vision

By :

KOBLI Mohammed badreddine

Defended publicly on 15/10/2025

In front of the jury :

BEKKAR Belgacem	MCA	Univ. Ghardaïa	**President**
Biteur Kada	MCB	Univ. Ghardaïa	**Examiner**
BEN CHAABANE Achour	MCB	Univ. Ghardaïa	**Examiner**
HACENE Nacer	MCA	Univ. Ghardaïa	**Supervisor**

Academic year 2024/2025

`Acknowledgment

All praises and thanks to Almighty ALLAH, the most beneficent and the most merciful, who gave us all abilities and helped us to complete this humble work.

I would like to express my sincere gratitude to my supervisor HACENE Nacer for his support and guidance during the course of this work. His encouragement and guidance have always been a source of motivation. It was an honor to work under his supervision.

Special thanks go to our professors, academic staff, and personnel at the University of Ghardaia.

Most importantly, I am grateful to my family who supported me every time I was in need, always standing by me and guiding me through life. I would like to thank them for their unconditional love that motivates me to aim higher.

Thanks

ملخص

تقدم هذا المذكرة نظام طائرة مسيرة ذكية مزودة برؤية بصرية وحرارية مزدوجة للتفتيش الذاتي لصوامع القمح. تم إنشاء نموذج ديناميكي للطائرة الرباعية ومقارنة أنظمة التحكم PID والتحكم الانزلاقي المتقدم (SMC) ، حيث أثبت الأخير تفوقه في تتبع المسار. كما تم تطوير نظام كشف عن العيوب يعتمد على الذكاء الاصطناعي باستخدام مجموعة بيانات مخصصة ونموذج شبكة عصبية إلتفافية CNN تم تدريبه عبر منصة Teachable Machine لتحديد مشاكل مثل الشقوق والصدأ. كما تم أيضا بناء نموذج أولي عملي ومعايرته، مما يثبت أن دمج التحكم المتقدم، وأجهزة الاستشعار ثنائية الرؤية، والذكاء الاصطناعي يُمكن من إجراء عمليات تفتيش شاملة وغير باضعة تعزز السلامة والكفاءة التشغيلية. يمهد هذا العمل الطريق لربط البحث النظري بالتطبيق العملي في إدارة البنية التحتية الحديثة.

الكلمات المفتاحية: الطائرات المسيرة الذكية، التصوير الحراري، التفتيش الذاتي، الذكاء الاصطناعي، صوامع القمح

Abstract

This master's thesis develops a smart drone system with normal and thermal vision for autonomous wheat silo inspection. It establishes a quadcopter dynamic model and compares PID and Sliding Mode Control (SMC), with SMC proving more robust for trajectory tracking. An AI-driven defect detection system was created using a custom dataset and a CNN model trained via Teachable Machine to identify issues like cracks and rust. A functional prototype was built and calibrated, demonstrating that the integration of advanced control, dual-vision sensors, and AI enables comprehensive, non-invasive inspections that improve safety and operational efficiency. This work bridges theoretical research and practical implementation for modern infrastructure management.

Keywords: Smart Drones, Thermal Imaging, Autonomous Inspection, Artificial Intelligence, Wheat Silos

Résumé

Ce mémoire de master développe un système de drone intelligent équipé de vision normale et thermique pour l'inspection autonome des silos à blé. Il établit un modèle dynamique de quadrirotor et compare les commandes PID par Mode Glissant (SMC), cette dernière s'avérant plus robuste pour le suivi de trajectoire. Un système de détection de défauts piloté par l'IA a été créé en utilisant un jeu de données personnalisé et un modèle de réseau neuronal convolutif entrainé via Teachable Machine pour identifier des problèmes tels que les fissures et la rouille. Un prototype fonctionnel a été construit et calibré, démontrant que l'intégration d'une commande avancée, de capteurs à double vision et de l'IA permet des inspections complètes et non invasives qui améliorent la sécurité et l'efficacité opérationnelle. Ce travail fait le lien entre la recherche théorique et la mise en œuvre pratique pour la gestion moderne des infrastructures.

Mots clés : Drones Intelligents, Imagerie Thermique, Inspection Autonome, Intelligence Artificielle, Silos à Blé.

Liste of figure

List of tables

List of Abbreviations

UAV	Unmanned Aerial Vehicle
CW	Clockwise
CWW	Counter Clockwise
PID	Proportional Integral Derivative
IoT	Internet of Things
VTOL	Vertical Take-Off and Landing
MALE	Medium Altitude Long Endurance
ADC	Analog to Digital Converter
ARM	Advanced RISC Machine
DOF	Degrees of Freedom
EKF	Extended Kalman Filter
ESC	Electronic Speed Control
GPS	Global Positioning System
HALE	High Altitude Long Endurance
IMU	Inertial Measurement Unit
I2C	Inter-Integrated Circuit
LiPo	Lithium Polymer Battery
Li-po	Lithium ion Battery
LPS22HB	Pressure Sensor
LQR	Linear Quadratic Regulator
MPC	Model Predictive Control
MPU6500	Motion Processing Unit
PPM	Pulse Position Modulation
PWM	Pulse Width Modulation
QMC5883L	3-Axis Magnetometer
ROI	Region of Interest
RSSI	Received Signal Strength Indicator

RS2205	RacerStar 2205 Motor
SBUS	Serial Bus
TS100	Digital Soldering Iron
UART	Universal Asynchronous Receiver-Transmitter
UKF	Unscented Kalman Filter
VRS	Vortex Ring State
AFHDS	Automatic Frequency Hopping Digital System
CSI	Camera Serial Interface
CNN	Convolutional Neural Network
DIP	Dual In-line Package
GCS	Ground Control Station
GAN	Generative Adversarial Network
GND	Ground
HDMI	High-Definition Multimedia Interface
MicroSD	Micro Secure Digital Card
RGB	Red Green Blue
ReLU	Rectified Linear Unit
RNN	Recurrent Neural Network
SDIO	Secure Digital Input Output
USB	Universal Serial Bus
VCC	Voltage Common Collect

Table of contents

General introduction

General introduction

The past decade has witnessed remarkable progress in the field of unmanned aerial vehicles (UAVs), particularly quadcopters, which have emerged as indispensable tools across a wide range of sectors owing to their flexibility, accuracy, and operational efficiency. These advanced aerial systems stand at the intersection of mechanical engineering, electronics, software, and artificial intelligence, rendering their design and control both a challenge and an opportunity for in- novation in modern engineering.

The present dissertation aims to provide a comprehensive study and a rigorous analysis of quadcopter systems, encompassing both theoretical and practical aspects. The research begins with the mathematical foundations of modeling and control, then advances toward practical implementation, with a particular emphasis on intelligent inspection tasks.

The work is structured in a coherent and sequential manner, where each chapter builds logically upon the foundations established in the preceding one.

The first chapter introduces UAVs with a particular focus on quadcopters, presenting their fundamental componentsincluding the frame, motors, sensors, and flight controllersalongside a review of their most impactful applications, such as precision agriculture, security monitoring, industrial inspection, and disaster management.

The second chapter addresses the mathematical modeling of the quadcopter. A complete nonlinear dynamic model is derived using the Newto- nEuler formalism to capture the relationship between control inputs and vehicle motion, followed by model simplification around the hovering equilibrium point and reformulation in state-space representation.

Chapter three examines the design and assessment of a classical yet effec- tive control strategy, namely the Proportional Integral Derivative (PID)

controller. A cascaded control architecture is adopted, wherein inner loops stabilize attitude dynamics while outer loops ensure trajectory tracking in three-dimensional space. The controllers performance is evaluated through simulations under diverse reference inputs.

Chapter four extends the control analysis to advanced nonlinear techniques by introducing Sliding Mode Control (SMC). Based on Lyapunov stability theory, sliding surfaces and control laws are formulated, and the results are compared against those of PID control to highlight improvements in robustness, accuracy, and dynamic response.

The fifth chapter shifts the focus from flight dynamics to intelligent applications, investigating the use of quadcopters in automated silo inspection. Leveraging image processing and artificial intelligence, particularly artificial neural networks, the system is designed to autonomously identify structural defects such as cracks and corrosion. A simplified machine learning workflow is demonstrated through the use of the Teachable Machine platform. Finally, the sixth chapter presents the practical implementation and prototyping stage. This includes the selection and integration of hardware components, programming of the flight controller (MiniPix) via Mission Planner, sensor calibration, and the incorporation of a Raspberry Pi board for onboard execution of computer vision algorithms.

By integrating theoretical modeling, advanced control design, and intelligent inspection applications, this dissertation aspires to bridge the gap between conceptual research and real-world implementation. The outcomes contribute to the advancement of autonomous aerial systems capable of performing complex tasks with efficiency, reliability, and adaptability in practical environments.

Chapter I : Quadcopter

Unmanned Aerial Vehicles :

An unmanned aerial vehicle (UAV), also known as a drone, is an aircraft with no or no human crew on board. They can be controlled remotely by a ground operator or operated autonomously using pre-programmed flight plans and on-board sensors. These aircraft received early, rapid and widespread adoption for military purposes. As these military systems have matured, a number of types of UAV systems with various on-board sensors have been developed for civilian applications, such as homeland security, wildfire monitoring, rapid response measurements for emergency disasters, earth science research, volcanic gas sampling, and humanitarian monitoring, biosensing/chemical/demining missions, and gas pipeline monitoring. Recent advances in the vehicles themselves and their associated sensor systems increase the attractiveness of these platforms to the geoscience community. Adaptable UAV platforms and imaging and sensing systems facilitate unique Earth observation capabilities for research and operational monitoring. [1]

I.1 Types of Unmanned Aerial Vehicles (UAVs) :

UAVs (drones) are classified according to their design, purpose, and operational range. Below are the main types :

1. **Based on Structure and Design :**
   - Fixed-Wing UAVs
   - Rotary-Wing UAVs
   - Hybrid UAVs (VTOL Drones)
2. Based on Size and Range :
   - Tactical UAVs
   - MALE (Medium Altitude Long Endurance)
   - HALE (High Altitude Long Endurance)

— Loitering Munition (Suicide Drones)

3. **Based on Application :**

— Military UAVs

— Commercial UAVs

— Research & Experimental UAVs

I.2 Quadcopter

Quadcopters feature a four-rotor design and are a dynamic class of unmanned aerial vehicles (UAVs) that leverage advanced technologies in aerodynamics, electronics, and mechanics. This unique configuration provides superior stability and maneuverability compared to traditional single-rotor helicopters, making them ideal for a range of applications, from aerial photography to precision agriculture and emergency response.[2]

A number of manned designs emerged in the 1920s and 1930s. These vehicles were among the first heavier-than-air vehicles to successfully perform vertical takeoff and landing (VTOL). However, early prototypes suffered from poor performance. With the development of electronic technology, such as advances in flight control computers, microprocessors, motors, high-efficiency batteries, advanced cameras, accelerometers, and global positioning systems, quadcopters have become more efficient and easier to use, making them accessible to a wider range of users.

The quadcopter's simple shape and design have made it increasingly popular in a variety of fields, including transportation, rescue, and photography. These drones are used for flying and maneuvering in tight spaces to capture innovative aerial photography, and their 3D appearance, beauty, and visual appeal are enjoyed by aerial photography and videography enthusiasts and professionals alike.

I.3 Components of U.A.V. (Quadcopter)

I.3.1 Quadcopter Frame

- X-Frame : The motors are of equal dimensions forming an x.
- H-Frame : Wider than an X-frame, with more space for mounting compo- nents.
- + Frame : Motors form a "+" shape instead of an "X."
- Deadcat Frame : Front arms are wider apart than rear arms.

I.3.2 Motor brushless

The motors are positioned in a way that allows the controller to rotate them easily. Because of their rotation, drones may move in a controlled manner. The motor a drone uses has a direct impact on its effectiveness.

I.3.3 Electronic speed control

An electronic speed control (ESC) is an electronic circuit that controls and regulates the speed of an electric motor. It may also provide reversing of the motor and dynamic braking. Miniature electronic speed controls are used in electrically powered radio controlled models. Full-size electric vehicles also have systems to control the speed of their drive motors[3].Each opposite two moves in the same direction and the other two are opposite CCW,CW

I.3.4 Propellers

The propellers (props) of your aircraft take the rotational energy of the spinning motor and turn that into lift. The props are usually the easiest item to change when it comes to fine tuning the performance of your propulsion system.[4]

I.3.5 Flight/board control

The quadcopter's flight controller is the point of contact between the device and the user. Any information you enter into the transmitter is transmitted to the aircraft via the flight controller[5]. This is controlled via a small circuit board for various uses, such as sensing and actuators.

I.4 Transmitter and receiver

Radio Transmitter and Receiver : These components are essential for control- ling your quadcopter. The transmitter is your remote control, while the receiver is mounted on the drone. They must operate on the same frequency and be compatible with your flight controller .[6]

I.5 Battery

The drone needs electric power to operate and throu gh battery type The duration of flight is determined and the amount of energy consumption is re-chargeable and there are two famous types of battery LiPo and Li-ion

I.6 Camera and Video

The camera is one of the most important parts of a drone when used for aerial photography or drone filming. Although not all drones have this element, it is one of the most common accessories, so the body of the drone usually has the necessary structure to install a camera on its base.[7]

I.7 GPS Module

GPS plays a pivotal role in providing drones with precise positioning and

navigation capabilities. GPS is a satellite-based navigation system that enables drones to accurately determine their location in real time. Drones equipped with GPS units can leverage this technology to accurately navigate way points, enabling them to follow predetermined routes or reach specific destinations with high accuracy.[8]

I.8 Application

I.8.1 Agriculture

The use of drones is growing rapidly in almost all sectors of the economy, but their use in the agricultural sector is booming.Drones can fly autonomously with dedicated software which allows making a flight plan and deploying the system with GPS and feed in various parameters such as speed, altitude, ROI (Region of Interest), geo-fence and fail-safe modes. Drones are preferred over full size aircrafts due to major factors like combination of high spatial resolution and fast turnaround capabilities together with low operation cost and easy to trigger. These features are required in precision agriculture where large areas are monitored and analyses are carried out in minimum time. Using of aerial vehicle is possible due to miniaturization of compact cameras and other sensors like infrared and sonar.[9]

FIGURE I.1 – Drone sprayer

I.8.2 Surveillance and security

Any drone off the shelf could be used as a security drone. Simply put, if youre putting a drone in the air to monitor a site and keep it safe, then that droneregardless

of how expensive it is, or what types of sensors it carriescould be called a security drone.[10]

FIGURE I.2 – Drone surveillance and security

I.8.3 Inspection Industrielle

drones have proven their effectiveness as tools, allowing us to capture close-up videos and images of suspected areas under restrictions, resulting in complete isolation. Whether it's for a routine health check or an emergency response, the goal is the same : to gather critical information that informs effective decisions regarding repairs and maintenance[11]. Their goal is to collect and analyze information such as temperature and humidity, guiding the selection of the best possible solutions.

FIGURE I.3 – Drone Inspection

I.8.4 rescue and disaster management

use of drones in disasters has the following benefits : they reduce the time required to locate victims and the time required for subsequent intervention by searching a wide area in a short period of time, in addition to the ability to search for victims and provide important information to rescuers about the path

to be taken during search and rescue operations.[12]

FIGURE I.4 – Drones for rescue and disaster management

I.8.5 photography

Photography has become increasingly important in light of advanced technological developments, as it has been combined with drones, revolutionizing the film, television, news, and cinematography industries. This allows us to capture images from multiple angles and in high resolution to capture breathtaking scenes such as racing and adventures, enhancing the visual experience.

FIGURE I.5 – photography Drones

I.8.6 Transport and Logistics

The integration of drones into the logistics and transportation sectors holds great promise, as ongoing developments contribute to direct and efficient deliveries, particularly in remote areas, expanding flight ranges, and improving safety standards. Traditional ground logistics often faces traffic congestion, infrastructure constraints, and geographical barriers, hindering the timely delivery of me-

dical supplies[13]. Addressing these issues requires collaboration between drone operators, regulatory bodies, and local communities to establish frameworks that ensure safe and efficient drone operations.

FIGURE I.6 – Drones Transport and Logistics

I.8.7 Scientific Research

With the rapid advancement of drone technology, researchers are increasingly using these flying vehicles to collect data where traditional instruments and the human eye cannot reach. Thanks to their lightness, agility, and advanced sensors, drones offer new insights from their unique vantage points[14]. The integration of artificial intelligence has significantly advanced control methods, which have been adopted in numerous scientific applications.

I.9 Quadcopter Dynamics

Drone motion is classified into four types based on the motion relationship between the four propellers : thrust, pitch, roll, and yaw.

1. **Throttle** The up and down movement of the drone is called throttle If all four propellors run at normal speed, then the drone will move down If all four propellors run at a higher speed, then the drone will move up. by

2. **Pitch** The forward or backward movement of the drone is called pitch. Increasing the speed of the rear propellers moves forward, while increasing the

speed of the front propellers moves backward.

3. **Roll** This is the movement of a drone, tilting left or right, by increasing thrust on one side. If the right propellers rotate at high speed, it will move to the left. If the left propellers rotate at high speed, it will move to the right.

4. **Yaw** The rotation of the aircraft's head around the vertical axis (left or right) is called yaw. If the two counterclockwise propellers increase, the aircraft will move left, while if the two clockwise propellers increase, the aircraft will move right.

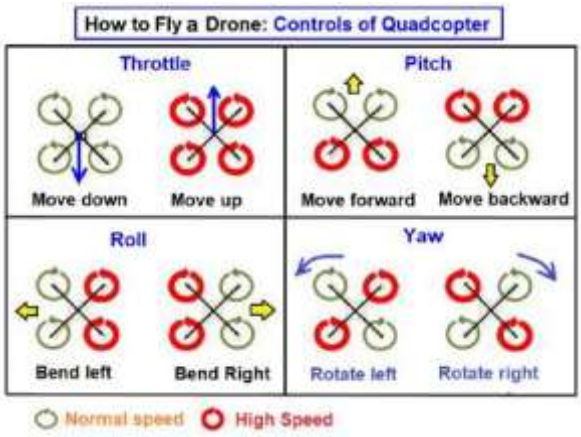

FIGURE I.7 – Quadcopter Dynamics

I.9.1 Forces and Moments Acting on a Drone

1. **lift** is generated by the downward force of air generated by the rotation of the drone's propellers, enabling the aircraft to climb or hover against gravity. The amount of lift depends on factors such as air density, blade design, and engine speed.

2. **Weight** The mass of a drone affects the direction of gravity. The heavier the drone, the greater the force required to lift and move it. Drone weight = drone mass Œ acceleration due to gravity.

3. **Thrust** This is the force that pushes the drone in a particular direction. It

is perpendicular to the plane of the rotor. During flight, the thrust is perfectly perpendicular. If the thrust is oblique, the drone will tilt forwards or backwards. This force is necessary to move the drone in the desired direction at an even speed.

4. **Drag** When a drone moves, it encounters air resistance, known as drag, which hinders its movement. Reducing drag is crucial to increasing efficiency and range. Streamlined designs and smooth surfaces help reduce drag.

I.10 Conclusion

Unmanned aerial vehicles (UAVs) have witnessed significant development and widespread interest in many fields, depending on their size, use, shape, and type. Drones are characterized by their ability to fly in difficult conditions, utilizing advanced technology in their manufacture and durability. The quadcopter's unique design and exceptional maneuverability have established it as a vital tool in diverse sectors, including transportation, emergency response, and aerial photography. Its ability to navigate in confined spaces and capture high-resolution images has transformed fields such as filmmaking, agriculture, and industrial inspection. The advancement of electronic technologiessuch as brushless motors, electronic speed controllers (ESCs), GPS units, and sophisticated flight controllershas greatly enhanced the functionality and accessibility of quadcopters, making them indispensable in both professional and recreational contexts, further enhancing their importance in modern society.

Chapter II :Modeling of a quadcopter

II.1 Introduction

Modeling constitutes a fundamental step in the study and control of aerial robotic systems. For quadcopters, which are inherently nonlinear, strongly coupled, and underactuated systems, the development of an accurate mathematical model is crucial to design effective control strategies.

This chapter provides a systematic derivation of the kinematic and dynamic models of a quadcopter based on classical mechanics. First, appropriate coordinate frames are defined to describe the vehicle's position and orientation in space. Then, the rotational transformations are formulated using Euler angles, followed by the derivation of the translational and rotational kinematic equations.

Subsequently, the NewtonEuler formalism is applied to obtain the complete dynamic model, which captures the relationship between the control inputs (thrust and torques) and the resulting motion of the vehicle. The resulting equations of motion form the theoretical foundation for control design, trajectory planning, and simulation in subsequent chapters.

II.2 Modeling

Modeling play a pivotal role in scientific research by providing virtual or scaled representations of real-world systems. Through mathematical models and computer simulations, researchers can study system behavior under various conditions, some of which may be dangerous or impractical to test in reality. The first step in any study is developing an accurate model : for a quadcopter, this involves both the kinematic model (which describes translational and rotational motions) and the dynamic model (which relates the dynamic forces and moments genera- ted by each rotor to the acceleration of the vehicle's center of mass). Practically, two main modeling frameworks are used : the Euler-Lagrange method and the Newton-Euler method. Each provides a systematic approach to derive equations

of motion and predict the quadcopter's response to control inputs and external disturbances.

II.3 Coordinate Frames

To model the motion of a quadcopter, it is essential to define appropriate coordinate frames that represent position and orientation. Typically, two main coordinate frames are used :

— **Inertial Frame :** A geographically fixed coordinate system. It describes the position and orientation of the quadcopter relative to its external environment, such as its altitude above the ground or its location. This frame is assumed to be stationary, making it a suitable reference for describing the overall motion of the aircraft.

— **Body Frame :** A coordinate system attached to the quadcopter's body, moving and rotating with it. This frame is used to describe the forces and moments acting on the quadcopter, such as the thrust generated by the propellers, as well as to calculate the angles (roll, pitch, yaw) and angular velocities[16].

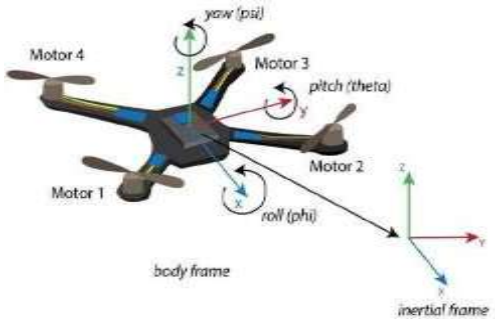

FIGURE II.1 – Inertial Frame and Body Frame

The orientation and motion of the quadcopter in three-dimensional space are described by transforming quantities between the Body Frame (attached to the aircraft) and the Inertial Frame (fixed to the ground).

II.4 Rotation Matrix Representation

The rotation of a quadrotor in three-dimensional space can be described in several ways : Euler angles, quaternions, Tait-Bryan angles, etc. The most widely used method in aerospace engineering is the Euler angle representation, which employs a Cartesian coordinate system for spatial rotation. The Euler angles are defined as follows :

— The roll angle ϕ represents a rotation about the x-axis ($-\pi/2 \leq \phi \leq \pi/2$).
— The pitch angle ϑ represents a rotation about the y-axis ($-\pi/2 \leq \vartheta \leq \pi/2$).
— The yaw angle ψ represents a rotation about the z-axis ($-\pi \leq \psi \leq \pi$).

II.4.1 Elementary Rotations

Transition from frame R_0 to frame R_i involves a rotation around the x-axis by the roll angle ϕ :

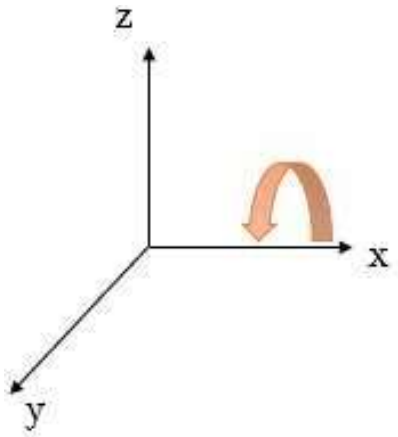

FIGURE II.2 – $R_x(\phi)$

$$R_x(\phi) = \begin{bmatrix} 1 & 0 & 0 \\ 0 & \cos\phi & -\sin\phi \\ 0 & \sin\phi & \cos\phi \end{bmatrix} \quad (1)$$

Next, the transition from frame R_i to frame R_j is a rotation about the y-axis by the pitch angle ϑ :

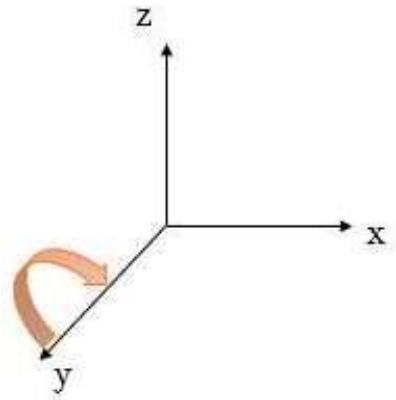

FIGURE II.3 – $R_y(\vartheta)$

$$R_y(\theta) = \begin{bmatrix} cos\ \theta & 0 & sin\ \theta \\ 0 & 1 & 0 \\ -sin\theta & 0 & cos\ \theta \end{bmatrix}$$

(2)

Finally, the transition from frame R_j to frame R_1 is a rotation about the z-axis by the yaw angle ψ :

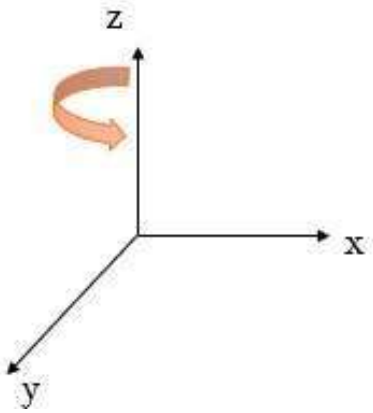

FIGURE II.3 – $R_z(\psi)$

$$R_z(\psi) = \begin{bmatrix} cos\ \psi & -sin\ \psi & 0 \\ sin\ \psi & cos & 0 \\ 0 & 0 & 1 \end{bmatrix}$$

(3)

The overall rotation matrix from R_1 to R_0 (or vice versa) is given by the successive product of the three basic rotations :

$$R(\phi, \vartheta, \psi) = R_z(\psi)R_y(\vartheta)R_x(\phi). \qquad (4)$$

Expanding this yields :

$$R = \begin{bmatrix} C_\psi C_\theta & S_\phi S_\theta C_\psi - C_\phi S_\psi & C_\phi S_\theta C_\psi + S_\phi S_\psi \\ S_\psi C_\theta & S_\phi S_\theta S_\psi + C_\phi C_\psi & C_\phi S_\theta S_\psi - S_\phi C_\psi \\ -S_\theta & S_\phi C_\theta & C_\phi C_\theta \end{bmatrix} \qquad (5)$$

where $C_k = \cos(k)$, $S_k = \sin(k)$.

II.5 Kinematics of the Quadcopter

The kinematics of the quadcopter describe the geometric relations between position, orientation and their time derivatives, without accounting for the forces and moments that produce the motion.

II.6 Generalized coordinates and velocities

Define the generalized position vector in the inertial frame :

$$\xi = [X \ Y \ Z \ \phi \ \theta \ \psi]^T \qquad (6)$$

and the generalized velocity vector expressed in the body frame :

$$\nu = [u \ v \ w \ p \ q \ r]^T \qquad (7)$$

where (u, v, w) are linear velocities along the body axes and (p, q, r) are the body angular rates about the x, y, z axes respectively.

II.6.1 Linear (translational) kinematics

The relation between the inertial-frame velocity of the center of mass and the body-frame linear velocity is given by the rotation matrix $R(\phi, \vartheta, \psi)$:

$$\begin{bmatrix} \dot{X} \\ \dot{Y} \\ \dot{Z} \end{bmatrix} = R(\phi, \theta, \psi) \begin{bmatrix} u \\ v \\ w \end{bmatrix} \qquad (8)$$

II.6.2 Rotational kinematics

Euler-angle rates are related to body angular rates by the kinematic transformation matrix T_Θ :

$$\begin{bmatrix} \dot{\phi} \\ \dot{\theta} \\ \dot{\psi} \end{bmatrix} = T_\Theta(\phi, \theta) \begin{bmatrix} p \\ r \\ q \end{bmatrix} \qquad (9)$$

$$T_\Theta(\phi, \theta) \begin{bmatrix} 1 & sin\phi\ tan\theta & cos\phi\ tan\theta \\ 0 & cos\ \phi & -sin\phi \\ 0 & \frac{sin\phi}{cos\theta} & \frac{cos\phi}{cos\theta} \end{bmatrix} \qquad (10)$$

valid for $|\vartheta| \neq \pi/2$ (i.e. away from pitch singularity).

II.6.3 Compact kinematic form

Combining translational and rotational kinematics, the full kinematic model is :

$$\dot{\xi} = J_\Theta(\phi, \vartheta, \psi)\, v \qquad (11)$$

where the Jacobian J_Θ is block-structured as

$$J_\theta(\phi, \theta, \psi) = \begin{bmatrix} R(\phi, \theta, \psi) & 0_{3*3} \\ 0_{3*3} & T_\theta(\phi, \theta, \psi) \end{bmatrix} \qquad (12)$$

Remark. Equation (11) is the link between the measured body velocities (from IMU/GPS fusion) and the time derivatives of the inertial pose. It is the natural interface between the geometric description of motion and the dynamic model that follows.

II.1 Dynamic Model

We now present the specific dynamic model of the quadrotor architecture, starting from the generic 6-DOF rigid-body equations derived using the Newto-nEuler formalism.

II.1.1 Newton Euler Equations

Two reference frames are defined :

— The inertial frame (E-frame), fixed to the Earth.

— The body frame (B-frame), fixed to the quadrotor structure.

The equations of motion are more conveniently expressed in the body frame due to the following advantages :

— The inertia matrix remains constant over time.

— Body symmetry simplifies the equations.

— Onboard measurements are naturally expressed in the body frame.

— Control forces are almost always defined in the body reference. The generic 6-DOF rigid-body kinematics are expressed as :

$$\dot{\xi} = J_\theta \, \nu, \qquad (13)$$

where ξ is the generalized position vector in the inertial frame, ν is the generalized velocity vector in the body frame, and J_Θ is the generalized transformation matrix.

The generalized position vector is defined as :

$$\xi = \begin{bmatrix} \Gamma_E \\ \theta_E \end{bmatrix} = [X \; Y \; Z \; \phi \;\; \theta \; \psi \;]^T \qquad (14)$$

where Γ_E is the position in the inertial frame and Θ_E the Euler angles.

$$\xi = \begin{bmatrix}\Gamma_E \\ \theta_E\end{bmatrix} = [X\ Y\ Z\ \phi\ \ \theta\ \psi\ ]^T \qquad (15)$$

The generalized velocity vector in the body frame is

where V_B is the linear velocity and ω_B the angular velocity.

The transformation matrix is structured as :

$$J_\theta = \begin{bmatrix} R & 0_{3*3} \\ 0_{3*3} & T_\theta \end{bmatrix} \qquad (16)$$

where R is the rotation matrix (Eq. 5) and T_Θ is the Euler angle transformation matrix :

$$T_\theta = \begin{bmatrix} 1 & S_\phi T_\theta & C_\phi T_\theta \\ 0 & C_\phi & -S_\phi \\ 0 & S_\phi / C_\theta & C_\phi C_\theta \end{bmatrix} \qquad (17)$$

The rigid-body dynamics including inertia m and inertia matrix I are :

$$\begin{bmatrix} F_B \\ \tau_B \end{bmatrix} = \begin{bmatrix} mI_{3*3} & 0_{3*3} \\ 0_{3*3} & I \end{bmatrix} \begin{bmatrix} \dot{V}_B \\ \dot{w}_B \end{bmatrix} + \begin{bmatrix} w_B * (mV_B) \\ w_B * (Iw_B) \end{bmatrix} \qquad (18)$$

where F_B and τ_B are the control forces and torques in the body frame.

II.2 Complete Dynamic Model

Following the standard assumptions (center of mass at origin, principal inertia axes aligned with body axes), the dynamic model of the quadrotor can be expressed as :

$$M_B \dot{v} + C_B(v)\, v = G_B(\xi) + O_B(v)\, \Omega + E_B \Omega^2, \qquad (19)$$

where M_B is the massinertia matrix, C_B the Corioliscentrifugal matrix, G_B the gravity contribution, O_B the gyroscopic contribution, and E_B the input distribution matrix.

Expanding this yields the translational and rotational equations of motion :

$$\begin{cases} \ddot{X} = \left(S_\psi S_\phi + C_\psi S_\theta C_\phi\right)\frac{U_1}{m} \\ \ddot{Y} = \left(-C_\psi S_\psi + S_\psi S_\theta C_\phi\right)\frac{U_1}{m} \\ \ddot{Z} = -g + \left(C_\theta C_\phi\right)\frac{U_1}{m} \\ \dot{p} = \frac{I_{yy}-I_{xx}}{I_{xx}} qr - \frac{J_{TP}}{I_{xx}} q\Omega + \frac{U_2}{I_{xx}} \\ \dot{q} = \frac{I_{zz}-I_{xx}}{I_{yy}} qr - \frac{J_{TP}}{I_{yy}} q\Omega + \frac{U_2}{I_{yy}} \end{cases}$$

$$\dot{r} = \frac{I_{xx}-I_{yy}}{I_{xx}} pq + \frac{U_4}{I_{zz}}$$

where U_1, U_2, U_3, U_4 are the collective thrust and control torques, defined as :

$$\begin{aligned} U_1 &= b(\Omega_1^2 + \Omega_2^2 + \Omega_3^2 + \Omega_4^2) \\ U_2 &= bl(\Omega_4^2 - \Omega_2^2) \\ U_3 &= bl(\Omega_3^2 - \Omega_1^2) \\ U_4 &= b(-\Omega_1^2 - \Omega_2^2 - \Omega_3^2 + \Omega_4^2) \end{aligned} \qquad (21)$$

with b the thrust factor, d the drag factor, l the arm length, and Ω_i the propeller angular speeds.

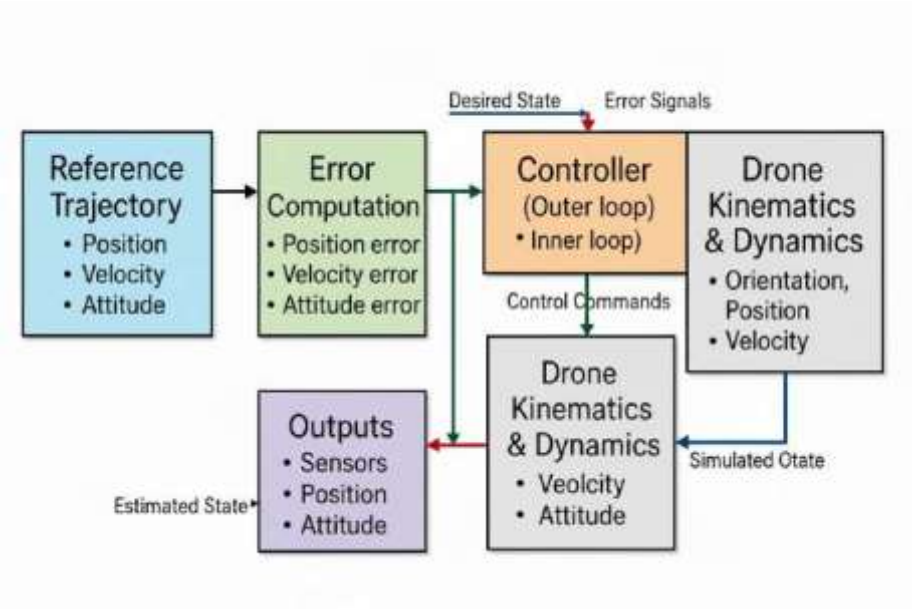

FIGURE II.5 – Block Diagram of Quadrotor Dynamics Model

II.3 Conclusion

In this chapter, a comprehensive mathematical foundation for quadcopter modeling was established. Beginning with the definition of appropriate coordinate frames, the transformation between the inertial and body frames was derived, allowing the description of motion in three-dimensional space. The kinematic model was then formulated, linking translational and rotational motion to body-frame velocities and angular rates. Subsequently, the dynamic model was developed based on Newton Euler principles, capturing how rotor-generated forces and torques influence both linear and angular accelerations of the quadcopter.

To facilitate control design, the nonlinear dynamics were linearized around the hover equilibrium point using small-angle approximations. This yielded simplified relations between translational accelerations and attitude angles, as well as between angular accelerations and control torques. The resulting linearized equations revealed the coupling between position and attitude, which is a key

insight for designing cascaded control architectures.

Finally, the system was expressed in state-space form, with clearly defined state and input vectors, and the associated matrices (A, B, C, D). This representation provides a compact and structured model that serves as the basis for modern control design and simulation. Overall, the derived framework bridges the gap between physical dynamics and control implementation, ensuring that subsequent chapters can focus on controller synthesis(PID).

Chapter III :PID control for stablisation and trajectory tracking

Introduction

Quadrotors have emerged as one of the most widely used aerial vehicles due to their mechanical simplicity, agility, and ability to operate in constrained environments. However, their dynamics are inherently unstable and strongly nonlinear, with highly coupled translational and rotational motions. This instability poses significant challenges for achieving both attitude stabilization and accurate trajectory tracking.

To address these challenges, classical control strategies remain attractive due to their simplicity and robustness. Among them, the ProportionalIntegralDerivative (PID) controller is still the most popular solution for quadrotors, both in academic research and industrial applications. The PID controller plays an important role in compensating for disturbances, reducing steady-state errors, and providing adequate damping, making it suitable for both linearized and nonlinear representations of quadrotor dynamics.

In this chapter, the PID controller will be designed and evaluated based on the previously derived linearized model of quadrotor dynamics, which simplifies the nonlinear and coupled system into decoupled rotational and translational equations. Using this simplified model, cascaded PID loops will be developed to stabilize the attitude (roll, pitch, and yaw) as well as to ensure trajectory tracking in three-dimensional space. The objectives of this chapter are therefore fourfold :

1. Highlight the importance of controlling the stability of quadrotors and ensuring accurate trajectory tracking.
2. Provide a concise overview of the instability problems arising from nonlinear and coupled dynamics.
3. Introduce the fundamental role of PID control in both linear and nonlinear systems.
4. Design and evaluate PID controllers for both stabilization and trajectory

tracking using the derived mathematical model.

III.1 PID Control Fundamentals

PID controllers are among the most common control systems used in indus- try. This is mainly because of their relatively simple structure, which makes them easy to understand and apply in practice. Their wide use has encouraged researchers and engineers to focus on improving their design and tuning in order to achieve better performance of control systems[19].

III.1.1 Formulation of the PID Controller

The ProportionalIntegralDerivative (PID) controller is one of the most widely used control strategies in engineering systems. Its basic principle is to compute the control input $u(t)$ based on the control error $e(t) = r(t) - y(t)$, where $r(t)$ is the reference signal (setpoint) and $y(t)$ is the measured output.

III.1.2 Standard Form

The ideal PID controller can be expressed as :

$$u(t) = k_p e(t) + k_i \int_0^t e(\tau)d\tau + k_d \frac{de(t)}{d(t)} \qquad (22)$$

where : k_p : proportional gain,

— k_i : integral gain,

— k_d : derivative gain

III.1.3 Parameterized Form

Alternatively, the controller can be parameterized using the integral time constant T_i and the derivative time constant T_d :

$$u(t) = k_p \left((e(t) + \frac{1}{T_i} \int_0^t e(\tau) d\tau + T_d \frac{de(t)}{d(t)} \right) \quad (23)$$

III.1.1 Interpretation of Terms

— The **proportional term** acts on the present value of the error.

— The **integral term** accounts for the accumulation of past errors, effectively removing steady-state error.

— The **derivative term** predicts future error behavior by estimating its rate of change, thus improving damping and stability.

It is important to note that the control signal $u(t)$ is formed entirely from the error $e(t)$, with no explicit feedforward term. The structure of the PID controller is illustrated in Figure III.1.

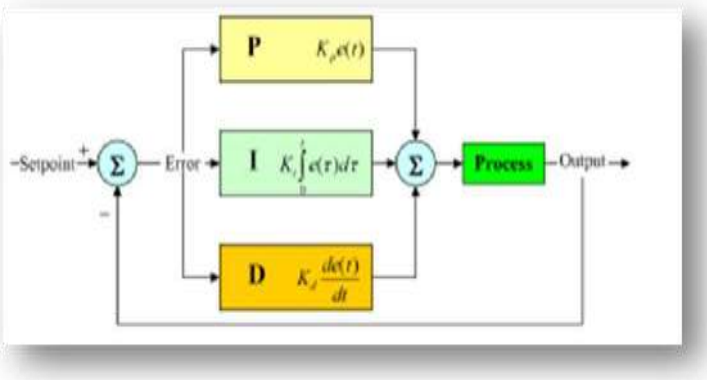

FIGURE III.1 – Block diagram of the PID controller (P, I and D branches) in a feedback loop.

,Full PID Behavior

The complete PID controller combines the benefits of proportional, integral, and derivative terms.

— Proportional : provides immediate response to error.

— Integral : ensures zero steady-state error.

— Derivative : anticipates error trends and improves damping.

Together, these effects make PID control a versatile and powerful tool for stabilizing quadrotor dynamics and achieving accurate trajectory tracking[20].

III.2 Simulation Results

III.2.1 PID for Attitude Stabilisation

The stabilization of a quadcopters attitude is achieved through an inner control loop that regulates the rotational dynamics around roll (ϕ), pitch (ϑ), and yaw (ψ). PID controllers are selected due to their simplicity, reliability, and good performance in many practical systems. Each attitude channel is controlled by an independent PID, which computes the required torque based on the error between the desired and actual angles.

The simplified linear model of the rotational dynamics around hover can be expressed as :

$$\ddot{\phi} \approx \frac{\tau_\phi}{I_{xx}}, \ddot{\theta} \approx \frac{\tau_\theta}{I_{yy}}, \ddot{\psi} \approx \frac{\tau_\psi}{I_{zz}}, \qquad (24)$$

where $\tau_\phi, \tau_\vartheta, \tau_\psi$ are the control torques generated by the rotors, and I_{xx}, I_{yy}, I_{zz} are the inertia components.

The general PID control law for an attitude channel $j \in \{\phi, \vartheta, \psi\}$ can

$$\tau_j(t) = K_{pj} e_{pj}(t) + k_{ij} \int_0^t e_j(\tau) d\tau + K_{dj} \frac{de_j(t)}{dt} \qquad (25)$$

where $e_j(t) = j_d(t) - j(t)$ is the tracking error between the desired and actual attitude angle.

For example, for roll control :

$$\tau_\phi(t) = K_{p\phi} e_\phi(t) + k_{i\phi} \int_0^t e_\phi(\tau) d\tau + K_{d\phi} \frac{de_j(t)}{dt} \qquad (26)$$

and similar expressions are applied to pitch (ϑ) and yaw (ψ).

In this structure, the proportional term (P) provides an immediate response to errors, the integral term (I) eliminates steady-state error, and the derivative term (D) improves damping and reduces overshoot. Together, these actions ensure robust attitude stabilisation of the quadcopter.

As shown in [21], the attitude of the quadrotor is stabilised using independent PID controllers in the inner loop of the cascaded control structure.

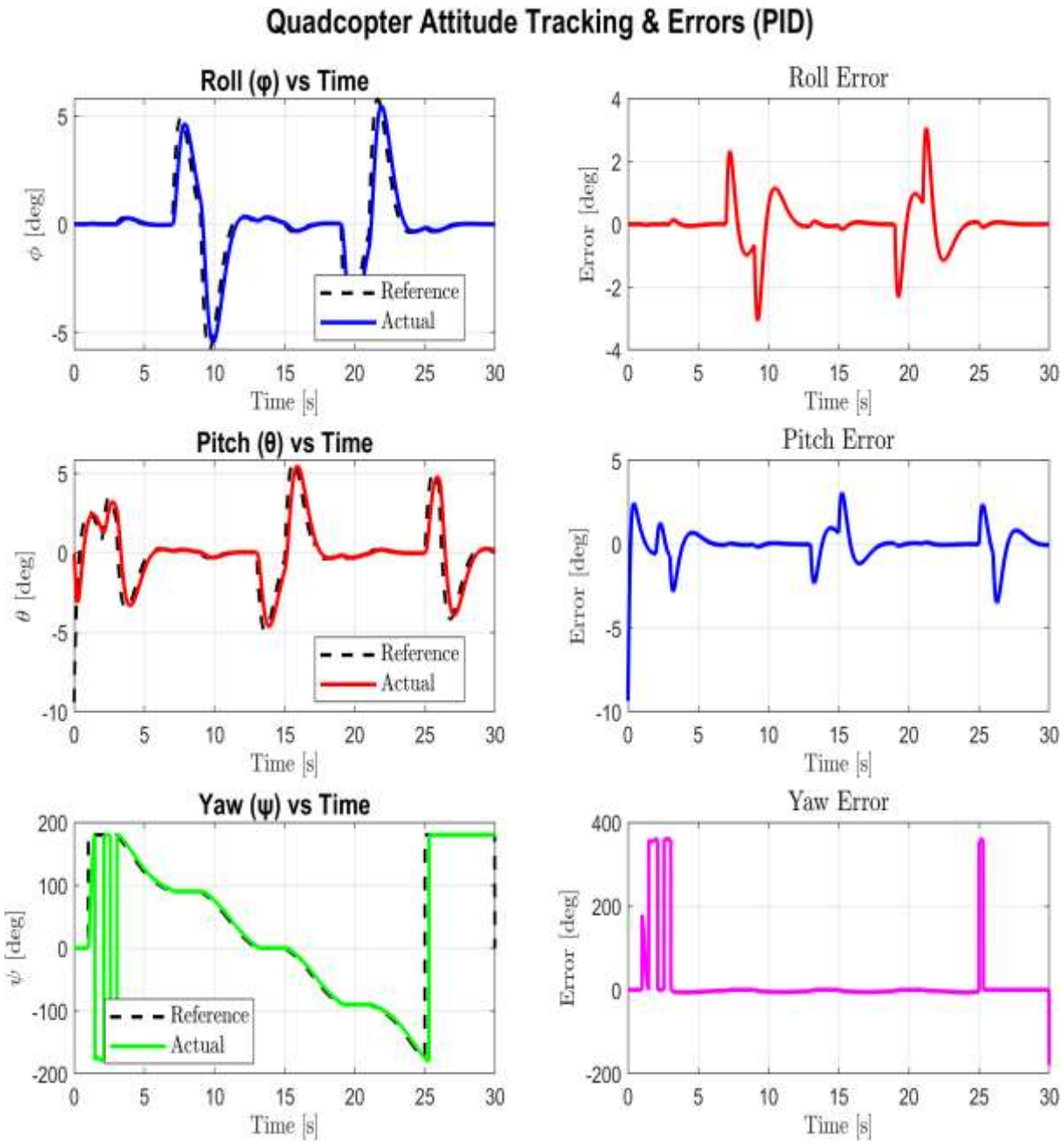

FIGURE III.2 – Attitude tracking and tracking errors (Roll, Pitch, Yaw) using PID controller

III.2.2 PID for Trajectory Tracking

In order to achieve accurate trajectory tracking for the quadrotor, a ProportionalIntegralDerivative (PID) controller is implemented. The main objective is to minimize the tracking error between the actual position of the quadrotor and the desired reference trajectory (straight line, circular path, or constant altitude).

The control law is defined as :

$$u(t) = K_p e(t) + K_i \int e(t)dt + K_d \frac{de(t)}{d(t)}$$

where :

- K_p : Proportional gain, responsible for reducing the instantaneous error.
- K_i : Integral gain, responsible for eliminating steady-state error.
- K_d : Derivative gain, responsible for predicting the future error and improving system stability.

To evaluate the performance of the controller, the following metrics are considered :

- **Tracking error** : Difference between reference trajectory and actual res- ponse.
- **Settling time** : Time required for the system to remain within a specific error bound.
- **Overshoot** : Maximum deviation from the reference trajectory during transients.

The controller gains used in the simulation are summarized in Table 1.

TABLE 1 – PID Gains for Quadcopter Control

Axis	**Position PID** (K_p, K_i, K_d)	**Attitude PID** (K_p, K_i, K_d)
X (Roll)	(3.5, 0.2, 2.5)	(6.0, 0.05, 1.5)
Y (Pitch)	(3.5, 0.2, 2.5)	(6.0, 0.05, 1.5)
Z (Altitude)	(6.0, 0.5, 3.5)	—
Yaw (ψ)	—	(4.0, 0.02, 0.8)

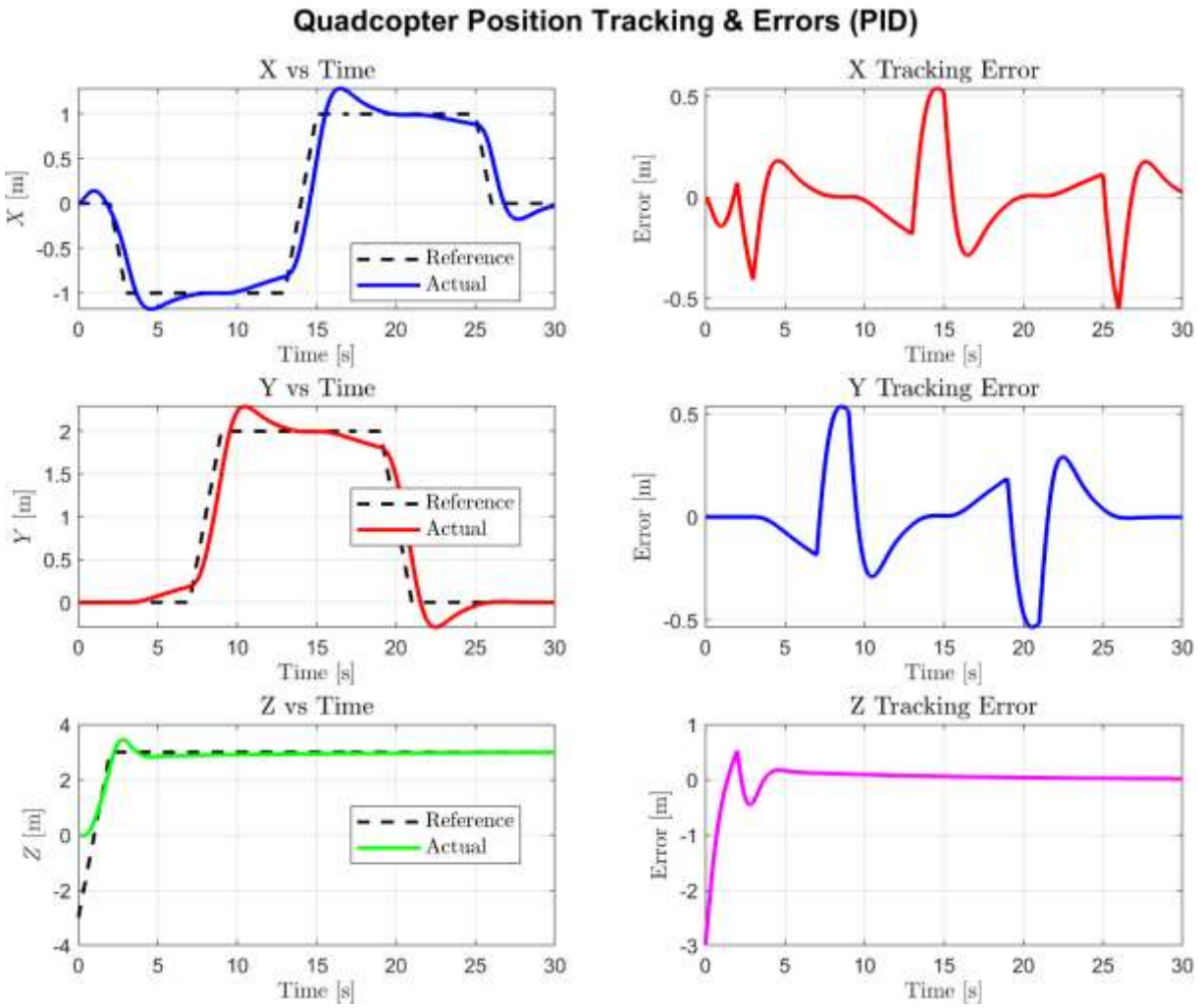

FIGURE III.4 – Position tracking and tracking errors using PID controller

Discussion

The obtained results demonstrate that the proposed cascaded PID structure provides robust stabilisation of both attitude and position. The inner loop guarantees fast angular tracking with minimal error, while the outer loop ensures precise trajectory following under different reference commands. Overall, the controller achieves a good balance between responsiveness, accuracy, and stability, validating its suitability for quadcopter applications.

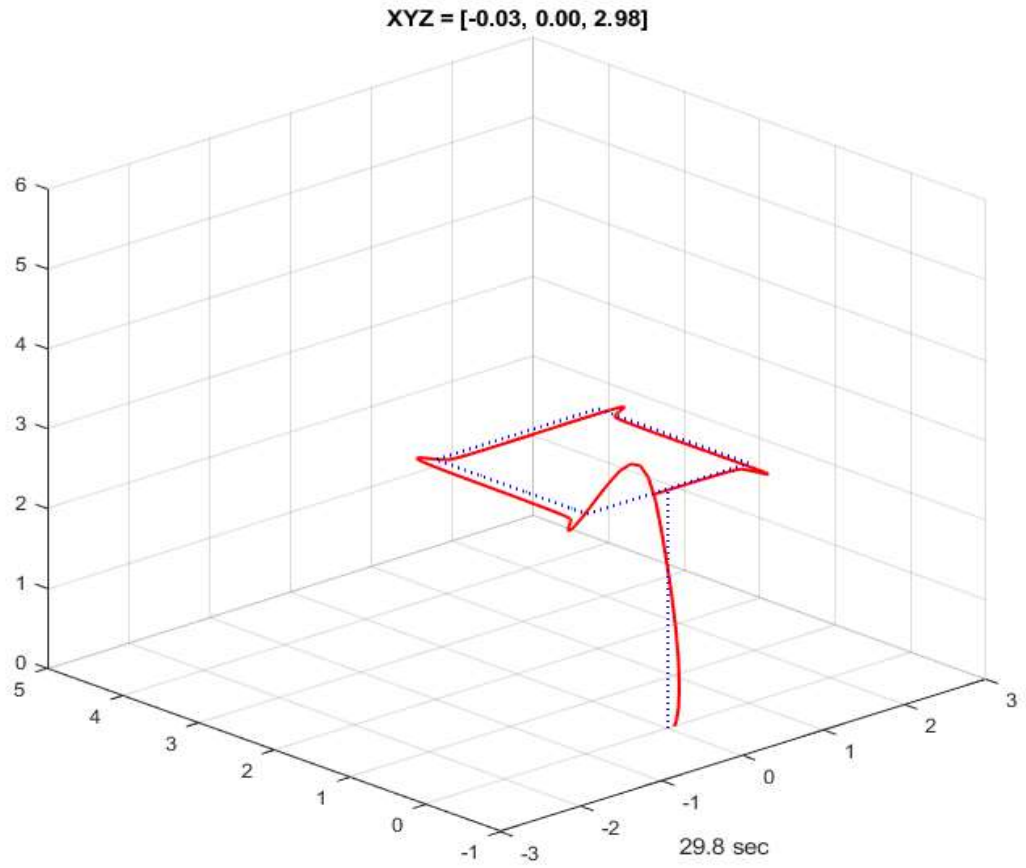

FIGURE III.5 – 3D Trajectory Tracking for a Drone using PID Control

III.1 Conclusion

In this chapter, the design and evaluation of cascaded PID controllers for quadrotor stabilisation and trajectory tracking were presented. The results showed that the PID-based structure provides satisfactory performance in terms of stability, disturbance rejection, and tracking accuracy. The inner attitude loop ensured fast and stable angular responses, while the outer position loop achieved reliable trajectory following with acceptable steady-state errors.

Despite these advantages, the limitations of PID controllers remain evident, particularly when dealing with strong nonlinearities, external disturbances, or model uncertainties. Since quadrotor dynamics are inherently nonlinear and subject to parameter variations, a more advanced and robust control approach becomes necessary.

To overcome these challenges, the next chapter introduces the *Sliding Mode Control* (SMC) strategy, which is well known for its robustness against disturbances and model uncertainties. By exploiting its nonlinear nature, SMC can enhance the performance and reliability of quadrotor control beyond the capabilities of classical PID methods.

Chapter IV :sliding mode control of a quadrotor for trajectory tracking

IV.1 Introduction

Quadrotor control remains a challenging problem due to the nonlinear, underactuated, and strongly coupled nature of its dynamics. Traditional linear controllers such as PID can achieve satisfactory performance in nominal conditions but may degrade in the presence of model uncertainties, parameter variations, and external disturbances such as wind gusts.

Sliding Mode Control (SMC) has emerged as a powerful nonlinear control technique to address these limitations. The key idea of SMC is to design a *sliding surface* in the state-space such that, once the system trajectory reaches this surface, the closed-loop dynamics exhibit desired behavior (e.g., stability and convergence to the reference). The controller consists of two components : an equivalent control that maintains the trajectory on the surface, and a switching control that drives the trajectory towards the surface in finite time.

In this section, we present the design of an SMC scheme for the quadrotor, including altitude, position, roll, pitch, and yaw subsystems. The control laws are derived based on Lyapunov stability theory to ensure exponential convergence of the sliding surfaces. Simulation results are then presented to demonstrate the performance of the proposed approach and to compare it with the classical PID control strategy.

IV.2 Sliding Mode Control

The quadrotor model is indeed complex and underactuated. As mentioned previously, the translational degrees of freedom (x, y) do not have direct control inputs. It is therefore necessary to introduce *virtual commands* (u_x, u_y) and apply a cascaded control structure similar to the one used with the PID controller .

We consider the full state vector of the system :

$$X = [x_1 \quad x_2 \quad x_3 \quad x_4 \quad x_5 \quad x_6 \quad x_7 \quad x_8 \quad x_9 \quad x_{10} \quad x_{11} \quad x_{12}]^T \qquad (27)$$

with :

$$x_1 = z, \qquad x_2 = \dot{z},$$

$$x_3 = x, \qquad x_4 = \dot{x},$$

$$x_5 = y, \quad x_6 = \dot{y},$$

$$x_7 = \phi, \quad x_8 = \dot{\phi},$$

$$x_9 = \vartheta, \quad x_{10} = \dot{\vartheta},$$

$$x_{11} = \psi, \quad x_{12} = \dot{\psi}.$$

can be rewritten in the state-space form :

$$\dot{X} = f(X, U) \qquad (28)$$

where the dynamic function $f(X, U)$ is given by :

$$f(X,U) = \begin{bmatrix} x_2 \\ g - \frac{\cos x_7 \cos x_9}{m} U_1 \\ x_4 \\ u_x \frac{1}{m} U_1 \\ x_6 \\ u_y \frac{1}{m} U_1 \\ x_8 \\ x_8 x_{12} a_1 + x_{10} a_2 \Omega_r + b_1 U_2 \\ x_{10} \\ x_7 x_{12} a_3 - x_8 a_4 \Omega_r + b_2 U_3 \\ x_{12} \\ x_{10} x_8 a_5 + b_3 U_4 \end{bmatrix} \qquad (29)$$

with the virtual controls (u_x, u_y) defined by :

$$\begin{cases} u_x = \cos\ \phi \sin\ \theta \cos\ \psi + \sin\ \phi \sin\ \psi \\ u_y = \cos\ \phi \sin\ \theta \sin\ \psi - \sin\ \phi \cos\ \psi \end{cases} \tag{30}$$

Finally, after generating the virtual commands (u_x, u_y) as shown in Figure III.2, we can compute the desired roll (ϕ_d) and pitch (θ_d) angles :

$$\begin{cases} \phi_d = \sin^{-1}\left(u_x \sin\ \psi - u_y \cos\ \psi\right) \\ \theta_d = \sin^{-1}\left(\dfrac{u_x \cos\ \psi - u_y \sin\ \psi}{\cos\ \phi}\right) \end{cases} \tag{31}$$

Principle of Sliding Mode Control Sliding Mode Control (SMC) is a robust control strategy designed to handle model uncertainties, unmodeled dynamics,

and disturbances. The control law is composed of two terms :

$$u_i = v_{i,eq} + v_{i,sw} \tag{32}$$

where the switching term is typically :

$$u_{i,sw} = k_i \text{sign}(s_i) + \eta_i s_i. \tag{33}$$

IV.2.1 Altitude (z) Control

To design a control law for the altitude subsystem, we first define the state tracking error e_1 and its derivative as follows :

$$e_1 = x_{1d} - x_1 \tag{34}$$

where x_{1d} is the desired altitude trajectory. The derivative of the error is given by :

$$\dot{e}_1 = \dot{x}_{1d} - x_2 \tag{35}$$

The sliding surface is then defined as :

$$s_1 = \dot{e}_1 + k_1 e_1 \tag{36}$$

where k_1 is a positive constant that satisfies the Hurwitz condition ($k_1 > 0$).

Differentiating (36), we obtain :

$$\dot{s}_1 = \ddot{e}_1 + k_1 \dot{e}_1 \tag{37}$$

To ensure stability, we introduce the Lyapunov candidate function :

$$V_1 = \frac{1}{2} s_1^2 \tag{38}$$

whose derivative is given by :

$$\dot{V}_1 = s_1 \dot{s}_1 \tag{39}$$

Substituting the system dynamics, we have :

$$\dot{V}_1 = s_1 \left(\ddot{x}_{1d} + \frac{\cos(x_7)\cos(x_9)}{m} U_1 - g - k_1 \dot{e}_1 \right) \tag{40}$$

The sliding mode controller is then designed as :

$$U_1 = \frac{m}{\cos(x_7)\cos(x_9)} (-\ddot{x}_{1d} + g - k_1 \dot{e}_1 - c_1 \text{sign}(s_1) - \eta_1 s_1) \tag{41}$$

With this control law, the Lyapunov derivative becomes :

$$\dot{V}_1 = s_1 \dot{s}_1 = s_1 \left(-\eta_1 s_1 - c_1 \text{sign}(s_1) \right) = -\eta_1 s_1^2 - c_1 |s_1| \leq -\eta_1 s_1^2 \tag{42}$$

Thus, we obtain :

$$\dot{V}_1 \leq -2\eta_1 V_1 \tag{43}$$

The solution of (42) is :

$$V_1(t) = e^{-2\eta_1 t} V_1(0) \tag{44}$$

Hence, in the Lyapunov sense, the sliding surface $s_1(t)$ converges exponentially to zero provided that $\eta_1, c_1 > 0$.

IV.2.2 Position X Control (u_x)

To design the sliding mode control law for the attitude subsystem, we start by defining the state tracking error e_2 and its derivative as :

$$e_2 = x_{2d} - x_2 \tag{45}$$

where x_{2d} represents the desired state trajectory. Its derivative is given by :

$$\dot{e}_2 = \dot{x}_{2d} - x_3 \tag{46}$$

The sliding surface for this subsystem is defined as :

$$s_2 = \dot{e}_2 + k_2 e_2 \tag{47}$$

where k_2 is a positive design parameter that satisfies the Hurwitz condition ($k_2 > 0$).

Differentiating (46), we obtain :

$$\dot{s}_2 = \ddot{e}_2 + k_2 \dot{e}_2 \tag{48}$$

To ensure system stability, the Lyapunov candidate function is chosen as :

$$V_2 = \frac{1}{2} s_2^2 \tag{49}$$

with its time derivative expressed as :

$$\dot{V}_2 = s_2 \dot{s}_2 \tag{50}$$

Considering the system dynamics, we obtain :

$$\dot{V}_2 = s_2\left(\ddot{x}_{2d} + f(x) + \frac{1}{I}U_2 - k_2\dot{e}_2\right) \tag{51}$$

where $f(x)$ represents the nonlinear terms of the dynamics and I is the inertia parameter.

The sliding mode control law is then proposed as :

$$U_2 = I(-\ddot{x}_{2d} - f(x) + k_2\dot{e}_2 - c_2\text{sign}(s_2) - \eta_2 s_2) \tag{52}$$

Substituting (51) into (??), we obtain the Lyapunov derivative :

$$\dot{V}_2 = s_2\big(-\eta_2 s_2 - c_2\text{sign}(s_2)\big) = -\eta_2 s_2^2 - c_2|s_2| \leq -\eta_2 s_2^2 \tag{53}$$

Therefore :

$$\dot{V}_2 \leq -2\eta_2 V_2 \tag{54}$$

The solution of (53) is given by :

$$V_2(t) = e^{-2\eta_2 t}V_2(0) \tag{55}$$

Thus, in the Lyapunov sense, the sliding surface $s_2(t)$ converges exponentially to zero.

IV.2.3 Position Y Control (u_y)

For the yaw subsystem, the tracking error e_3 and its derivative are defined as :

$$e_3 = x_{3d} - x_3 \tag{56}$$

where x_{3d} denotes the desired yaw trajectory. Its derivative is given by :

$$\dot{e}_3 = \dot{x}_{3d} - x_4 \tag{57}$$

The sliding surface is defined as :

$$s_3 = \dot{e}_3 + k_3 e_3 \tag{58}$$

where k_3 is a positive constant satisfying the Hurwitz stability condition ($k_3 > 0$).

Differentiating (57), we obtain :

$$\dot{s}_3 = \ddot{e}_3 + k_3 \dot{e}_3 \tag{59}$$

The Lyapunov candidate function is chosen as :

$$V_3 = \frac{1}{2} s_3^2 \tag{60}$$

with its derivative expressed as :

$$\dot{V}_3 = s_3 \dot{s}_3 \tag{61}$$

Considering the dynamics of the subsystem, we have :

$$\dot{V}_3 = s_3 \left(\ddot{x}_{3d} + g(x) + \frac{1}{J} U_3 - k_3 \dot{e}_3 \right) \tag{62}$$

where $g(x)$ represents the nonlinear terms and J is the inertia parameter.

The sliding mode control law is then designed as :

$$U_3 = J(-\ddot{x}_{3d} - g(x) + k_3 \dot{e}_3 - c_3 \text{sign}(s_3) - \eta_3 s_3) \tag{63}$$

Substituting the control law into the Lyapunov derivative gives :

$$\dot{V}_3 = s_3 \big(-\eta_3 s_3 - c_3 \text{sign}(s_3) \big) = -\eta_3 s_3^2 - c_3 |s_3| \leq -\eta_3 s_3^2 \tag{64}$$

Thus :

$$\dot{V}_3 \leq -2\eta_3 V_3 \tag{65}$$

The solution is :

$$V_3(t) = e^{-2\eta_3 t} V_3(0) \tag{66}$$

Therefore, in the Lyapunov sense, the sliding surface $s_3(t)$ converges exponentially to zero if $\eta_3, c_3 > 0$.

For the roll control design, we begin by defining the state tracking error e_4 and its derivative :

$$e_4 = x_{7d} - x_7 \tag{67}$$

where x_{7d} is the desired roll (ideal position) signal. The time derivative of the error is

$$\dot{e}_4 = \dot{x}_{7d} - x_8 \tag{68}$$

The sliding surface is chosen as :

$$s_4 = \dot{e}_4 + k_4 e_4 \tag{69}$$

where $k_4 > 0$ is a design constant ensuring the Hurwitz condition.

Differentiating (68) yields :

$$\dot{s}_4 = \ddot{e}_4 + k_4 \dot{e}_4 \tag{70}$$

Select the Lyapunov candidate :

$$V_4 = \frac{1}{2} s_4^2 \tag{71}$$

so that

$$\dot{V}_4 = s_4 \dot{s}_4. \tag{72}$$

Using the subsystem dynamics (as provided), the Lyapunov derivative can be written as :

$$\dot{V}_4 = s_4(\ddot{x}_{7d} - x_8 x_{12} a_1 - x_{10} a_2 \Omega_r - b_1 U_2 + k_4 \dot{e}_4) \tag{73}$$

To make $\dot{V}_4$ negative semi-definite, choose the sliding-mode control law

$$U_2 = \frac{1}{b_1}(\ddot{x}_{7d} - x_8 x_{12} a_1 - x_{10} a_2 \Omega_r + k_4 \dot{e}_4 + c_4 \text{sign}(s_4) + \eta_4 s_4) \tag{74}$$

with design gains $c_4 > 0$ and $\eta_4 > 0$.

Substituting (72) into (73) gives

$$\dot{V}_4 = s_4\big(-\eta_4 s_4 - c_4 \text{sign}(s_4)\big) = -\eta_4 s_4^2 - c_4|s_4| \leq -\eta_4 s_4^2. \tag{75}$$

Therefore,

$$\dot{V}_4 \leq -2\eta_4 V_4 \tag{76}$$

and the solution of (75) is

$$V_4(t) = e^{-2\eta_4 t} V_4(0). \tag{77}$$

Hence, in the Lyapunov sense, the sliding surface $s_4(t)$ converges exponentially to zero provided that $\eta_4 > 0$ and $c_4 > 0$.

IV.2.4 Tangage Control ϑ

For the design of a sliding mode control law for the pitch subsystem (U_3), we first define the tracking error of the state x_9 and its derivative as :

$$e_5 = x_{9d} - x_9 \tag{78}$$

where x_{9d} represents the desired reference signal. The derivative of the error is expressed as :

$$\dot{e}_5 = \dot{x}_{9d} - x_{10} \tag{79}$$

The sliding surface of the controller is defined as :

$$s_5 = \dot{e}_5 + k_5 e_5 \tag{80}$$

where k_5 must satisfy the Hurwitz stability condition, i.e., $k_5 > 0$. From equation (79), we have :

$$\dot{s}_5 = \ddot{e}_5 + k_5 \dot{e}_5 \tag{81}$$

We choose the Lyapunov candidate function :

$$V_5 = \frac{1}{2} s_5^2 \tag{82}$$

and its time derivative is given by :

$$\dot{V}_5 = s_5 \dot{s}_5 \tag{83}$$

In order to guarantee $\dot{V}_5 < 0$, we write :

$$\dot{V}_5 = s_5(\ddot{x}_{9d} - x_7 x_{12} a_3 + x_8 a_4 \Omega_r - b_2 U_3 + k_5 \dot{e}_5) \tag{84}$$

To ensure that $\dot{V}_5$ is negative semi-definite, the control law U_3 is designed as :

$$U_3 = \frac{1}{b_2}[\ddot{x}_{9d} - x_7 x_{12} a_3 + x_8 a_4 \Omega_r + k_5 \dot{e}_5 + c_5 \text{sign}(s_5) + \eta_5 s_5] \tag{85}$$

Substituting this control input gives :

$$\dot{V}_5 = s_5\big(-\eta_5 s_5 - c_5 \text{sign}(s_5)\big) = -\eta_5 s_5^2 - c_5 |s_5| \leq -\eta_5 s_5^2 \tag{86}$$

Thus, we have :

$$\dot{V}_5 \leq -2\eta_5 V_5 \tag{87}$$

which leads to the solution :

$$V_5(t) = e^{-2\eta_5 t} V_5(0) \tag{88}$$

Therefore, according to Lyapunov stability theory, the sliding mode controller ensures that $s_5(t)$ converges exponentially to zero, provided that $\eta_5, c_5 > 0$.

IV.3 Yaw Control Law ψ

For the design of a control law for the yaw subsystem (U_4), we first define the state tracking error x_{11} and its derivative as follows :

For the design of a control law for the yaw subsystem (U_4), we first define the state tracking error x_{11} and its derivative as follows:

$$e_6 = x_{11d} - x_{11} \tag{89}$$

where x_{11d} is the desired reference signal. The derivative of the tracking error is given by :

$$\dot{e}_6 = \dot{x}_{11d} - x_{12} \tag{90}$$

The sliding surface of the controller is defined as :

$$s_6 = \dot{e}_6 + k_6 e_6 \tag{91}$$

where k_6 must satisfy the Hurwitz condition, i.e., $k_6 >$

0. From equation (90) , we obtain :

$$\dot{s}_6 = \ddot{e}_6 + k_6 \dot{e}_6 \tag{92}$$

We introduce the Lyapunov candidate function :

$$V_6 = \frac{1}{2} s_6^2 \tag{93}$$

Its time derivative is :

$$\dot{V}_6 = s_6 \dot{s}_6 \tag{94}$$

To ensure $\dot{V}_6 < 0$, we expand :

$$\dot{V}_6 = s_6(\ddot{x}_{11d} - x_{10} x_8 a_5 - b_3 U_4 + k_6 \dot{e}_6) \tag{95}$$

To make $\dot{V}_6$ negative semi-definite, the control law U_4 is chosen as :

$$U_4 = \frac{1}{b_3}[\ddot{x}_{11d} - x_{10}x_8a_5 + k_6\dot{e}_6 + c_6\text{sign}(s_6) + \eta_6 s_6] \tag{96}$$

Substituting back into the Lyapunov derivative :

$$\dot{V}_6 = s_6\dot{s}_6 = s_6\big(-\eta_6 s_6 - c_6\text{sign}(s_6)\big) = -\eta_6 s_6^2 - c_6|s_6| \leq -\eta_6 s_6^2 \tag{97}$$

Thus,

$$\dot{V}_6 \leq -2\eta_6 V_6 \tag{98}$$

The solution of (97) is :

$$V_6(t) = e^{-2\eta_6 t}V_6(0) \tag{99}$$

We can see, in the sense of Lyapunov theory, that the sliding mode controller ensures that $s(t) \rightarrow 0$ exponentially for $\eta_6, c_6 > 0$.

The derived control laws ensure exponential convergence of the sliding surfaces, guaranteeing robustness and stability of the closed-loop system. The design parameters $k_i, \eta_i, c_i > 0$ must be chosen to satisfy Lyapunov stability and performance requirements.

IV.3.1 SMC for Attitude and Trajectory Tracking

Sliding Mode Control (SMC) is a robust nonlinear control technique that is particularly well-suited for quadrotors due to its ability to handle model uncertainties and external disturbances. Unlike linear PID controllers, SMC is based on defining a *sliding surface* that combines both the error and its derivative, forcing the system dynamics to converge towards it.

For the position tracking, the sliding surface s_p is defined as :

$$s_p(t) = \dot{e}_p(t) + \lambda_p e_p(t) \tag{100}$$

where $e_p(t) = p(t) - p_d(t)$ is the position error vector, and $\lambda_p > 0$ is a design parameter that determines the convergence rate.

The control input for the translational dynamics can be expressed as :

$$F_{\text{des}} = m\left(\ddot{p}_d(t) - \lambda_p \dot{e}_p(t) - k_p \text{sat}\left(\frac{S_p}{\varepsilon}\right) + g\right), \qquad (101)$$

where $k_p > 0$ is the control gain, ε is a small positive constant for smoothing, and sat($\cdot$) is the saturation function.

Similarly, for the attitude dynamics, the sliding surface s_a is defined as :

$$s_a(t) = \dot{e}_a(t) + \lambda_a e_a(t), \qquad (102)$$

where $e_a(t) = \eta(t) - \eta_d(t)$ represents the error in Euler angles (ϕ, θ, ψ). The control law for the torques is then given by :

$$\tau = -I\lambda_a \dot{e}_a(t) - k_a \text{sat}\left(\frac{S_a}{\varepsilon}\right), \qquad (103)$$

with I being the inertia matrix and k_a the attitude control gain.

This structure ensures that both position and attitude errors converge towards zero while providing robustness against model uncertainties and disturbances.

Sliding Mode Control Parameters:

The sliding mode controller gains were tuned through simulation to ensure fast response and minimal chattering.

TABLE 2 – Sliding Mode Control Parameters

Parameter	*Symbol*	*Value*
Position sliding gain	λ_p	1.5
Position switching gain	k_p	5.0
Attitude sliding gain	λ_a	8.0
Attitude switching gain	k_a	3.0
Boundary layer thickness	ε	0.05

Here, λp and λa define the sliding surface slopes for position and attitude loops respectively, affecting convergence speed.

The gains kp and ka determine the control effort needed to reject disturbances, while ϵ defines the boundary layer thickness to mitigate chattering.

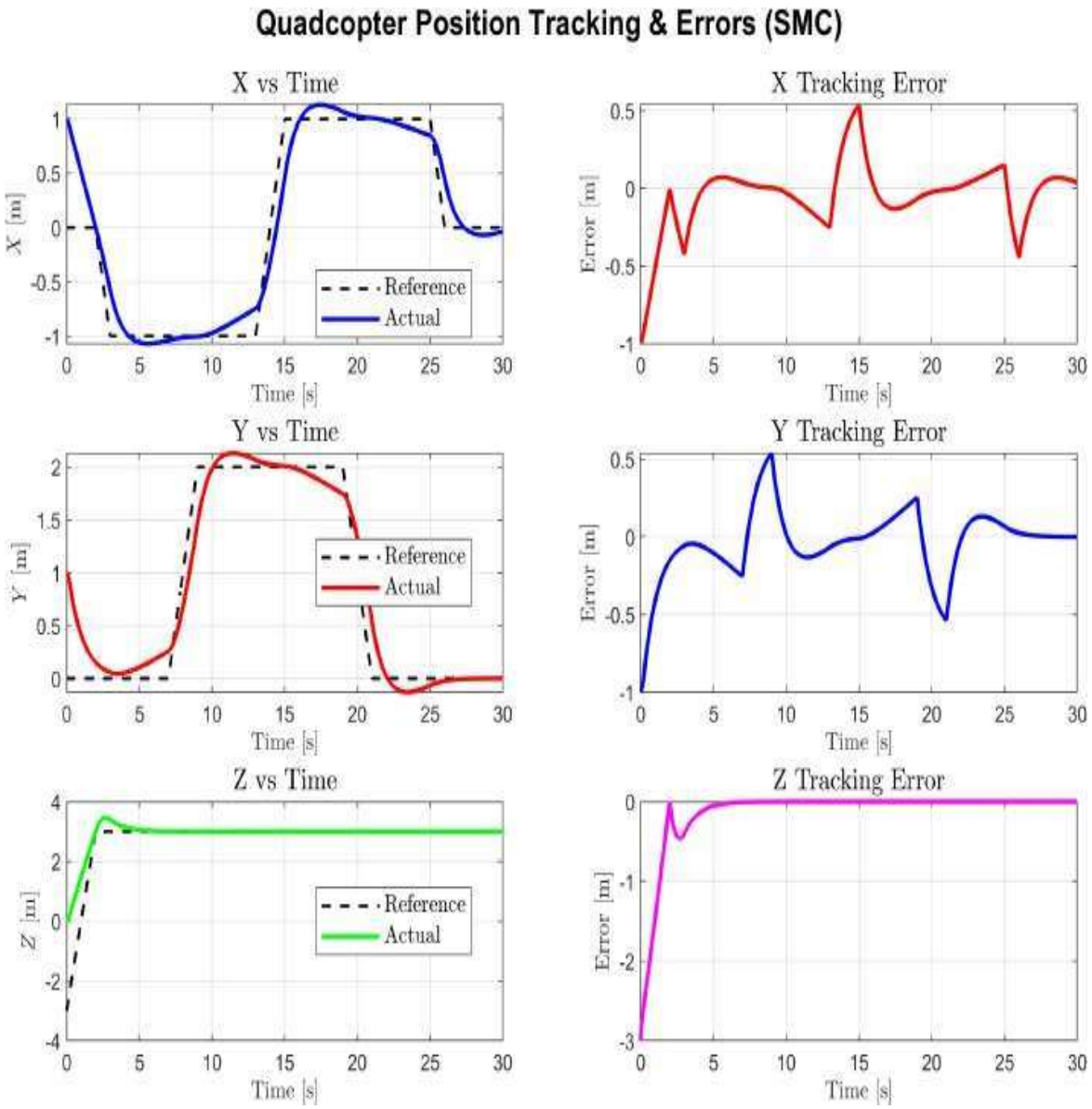

FIGURE IV.1 – Position tracking and tracking errors of the quadcopter using SMC

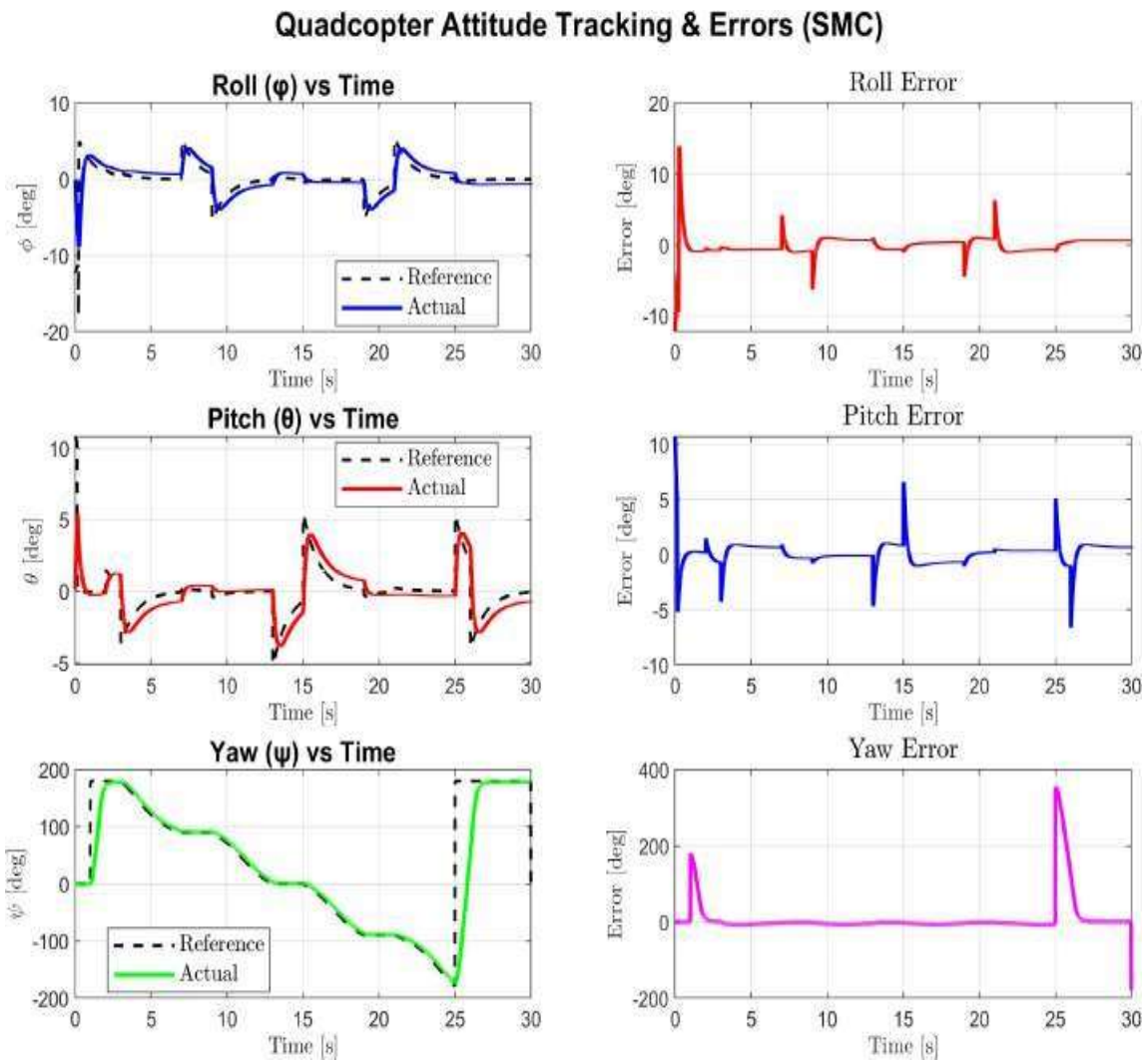

FIGURE IV.2 – Attitude tracking and tracking errors of the quadcopter using SMC.

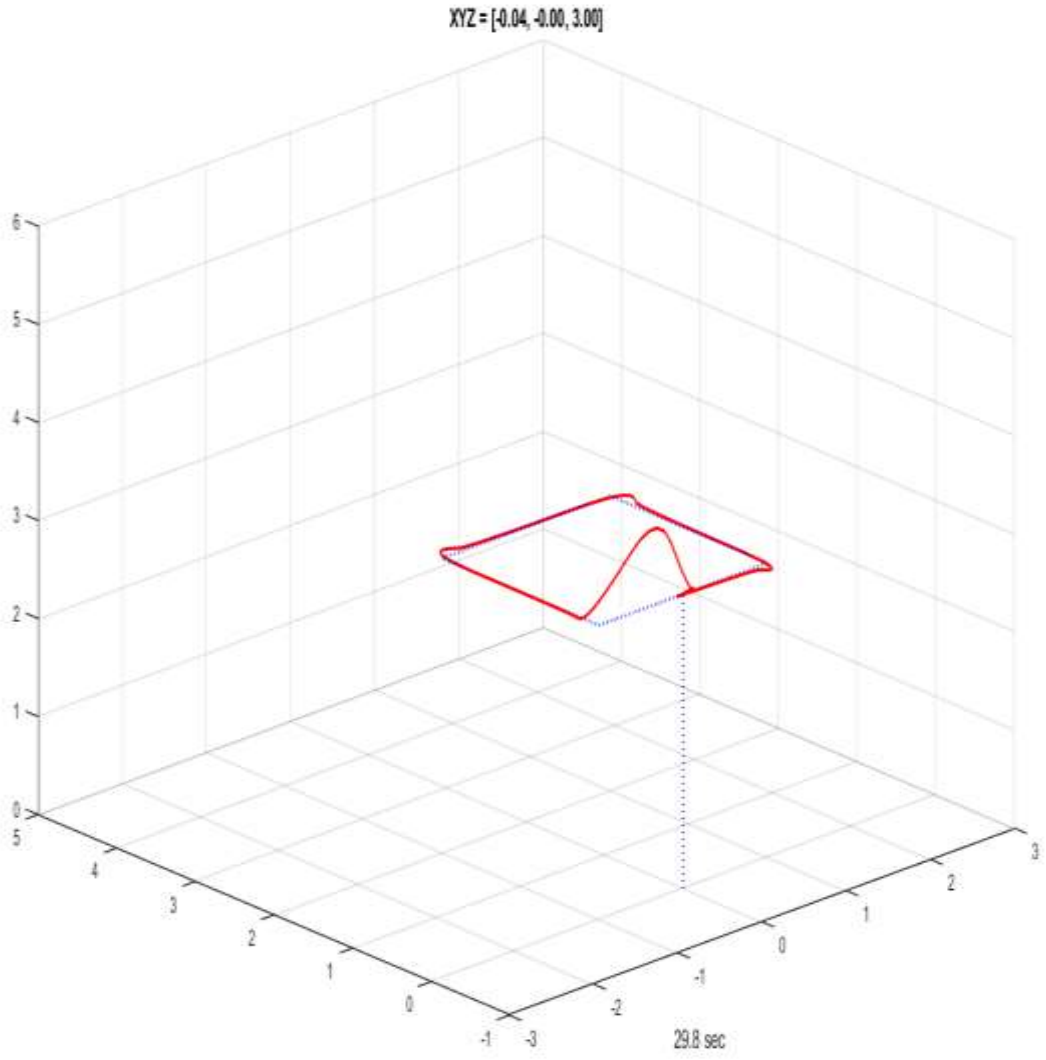

FIGURE IV.3 – 3D Trajectory Tracking for a Drone using Sliding Control

IV.3.2 Discussion

The obtained results confirm that the SMC strategy achieves fast and accurate tracking of both the trajectory and the attitude. Compared to the PID controller, SMC provides :

— **Improved robustness** against model uncertainties and unmodeled dynamics.

— **Smaller tracking errors**, especially during rapid trajectory changes.

— **Better disturbance rejection**, maintaining stability even under sudden reference variations.

Overall, SMC demonstrates superior performance for quadcopter control, making it an effective solution for real-world applications where robustness is critical.

TABLE 2 – Comparison between PID and Sliding Mode Control (SMC)

Criteria	**PID Controller**	**SMC Controller**
Disturbance Rejection	Moderate, performance can degrade under large disturbances.	High robustness against model uncertainties and external disturbances.
Response Speed	Moderate, depends on tuning of K_p, K_i, K_d.	Fast convergence due to sliding surface design.
Tuning Complexity	Simple, requires adjusting three gains.	More complex, requires designing sliding surface and control law.
Model Dependency	Sensitive to modeling errors.	Less sensitive, maintains stability despite modeling errors.
Chattering Effect	No chattering, smooth control signal.	May produce chattering; requires smoothing techniques (e.g., boundary layer).
Implementation	Easy and widely used in industry.	More computationally demanding, suitable for nonlinear systems.

IV.4 Conclusion

In this chapter, a comprehensive mathematical modeling of the quadrotor was presented, followed by the development of a Sliding Mode Control (SMC) strategy. The nonlinear and underactuated nature of the system was addressed by introducing virtual control inputs and employing a cascaded control structure to ensure trajectory tracking and attitude stabilization.

The design of the sliding surfaces and the corresponding control laws was carried out based on Lyapunov stability theory, guaranteeing convergence of the system states to the desired references despite parameter uncertainties and external disturbances. Compared to classical linear controllers, the proposed

SMC approach offers improved robustness, fast response, and reduced sensitivity to model inaccuracies.

This theoretical framework establishes a solid foundation for the subsequent simulation and experimental validation. The next chapter will focus on numerical simulations to evaluate the effectiveness and performance of the proposed control scheme under various operating conditions.

Chapter V :AI-based inspection of silos

V.1 Introduction

Wheat silo inspection is a critical task, directly impacting food safety, struc- tural integrity, and operational efficiency. Traditional inspection methods, which rely heavily on manual labor and human monitoring, often expose workers to significant risks and make the process susceptible to human error, in addition to being costly and time-consuming.

With the tremendous advancements in artificial intelligence (AI) and image processing technologies, a golden opportunity has emerged to automate this inspection process, increasing its accuracy and speed while reducing costs and risks. This section focuses on the first essential stage in building any smart system : data collection. We will explore the process of collecting a rich, labeled dataset of the most common defects in wheat silos, such as cracks, rust, and insect and rodent intrusion, using two sources : images captured during field training at the Algerian company Ammays and other images from open sources online. We will also discuss a methodology for using the Teachable Machine platform to classify this data and train a preliminary machine learning model, paving the way for building a smart inspection system based on computer vision.

V.2 Data Collection

Data collection is the systematic process of gathering, measuring, and analyzing information from various sources to answer research questions, test hypotheses, and evaluate outcomes. It ensures that researchers or decision-makers obtain accurate and reliable data to support conclusions, policy-making, or sys- tem improvements.[22]

V.2.1 Training Period at the Company

During the training period at the Amais Algeri Company, direct observations of the operation of the wheat silos were conducted. There are 12 silos arranged in two rows with a storage capacity of half a million quintals. During this training, the challenges facing steel silo inspection were studied, such as security risks, difficulty accessing high and internal areas.

When harvesting wheat or corn, the truck is initially received at a weighbridge, then goes through the cleaning process, separating stones and impurities, and then unloading it in a designated area. It is then transported via conveyors and elevators. Temperature, humidity, and fill levels are monitored and studied. The monitoring and control system includes periodic maintenance : motors, conveyor belts, air pumps, and mechanical gates. Fumigation and sterilization methods are also monitored to combat insects and fungi.

Through this field training, I learned about the general structure and functions of silos. I gained experience in understanding administrative methods for managing inventory, distributing wheat, and transporting it to mills, as well as monitoring the receiving, storing, and unloading processes. I also learned about monitoring systems, air distribution and ventilation methods, cleaning and separation processes to remove impurities, and preventive and corrective maintenance methods for equipment. Work teams were accompanied during the wheat receiving, weighing, initial inspection, and unloading.

FIGURE V.1 – Amayis algerie M'GUIDEN

V.2.2 Acquisition of images and measurements :

This is the first practical phase of inspection, where we capture and collect visual and digital data from the silo using advanced tools and techniques, rather than relying solely on human observation. The goal is to obtain accurate, quantitative, and comprehensive information to feed into artificial intelligence systems for processing, storage, and analysis. The dataset was built using two complementary sources :

Captured Images : Images were collected directly using a camera to simulate realistic inspection conditions. These images provide real-world visual data on defects as they appear in actual silos.

Online Images : Additional images were collected from open source platforms such as iStock and adobe stock and online image repositories. These images were used to enrich the dataset, especially in cases where direct collection of some defects was limited.

The images were classified into specific categories used to train the AI model, representing the most common defects and inspection targets in wheat silos :
Cracks : Structural fractures on silo walls or roofs. Rust : Deterioration of metal surfaces, particularly on roofs, joints, and ventilation structures.
Ventilation grilles : Images focused on ventilation openings, with a particular focus on blockages or damage that could impede airflow.
Insects : The presence of insects such as beetles, weevils, or mold that could contaminate stored grain.
Rodents : The presence of rodents in or near silos, posing health and structural risks.
Using Teachable Machine :
To simplify the classification process, the dataset was imported into Google Teachable Machine, a web platform that allows machine learning models to be trained without advanced programming requirements. By providing input data (images, sounds, or body postures), the system then generates a trained model that can be exported and run on a computer. The platform was used as follows :

1 Data loading : Images for each category (cracks, corrosion, ventilation grilles, insects, and rodents) were uploaded into separate categories.

2 Training : Teachable Machine automatically split the dataset into sub-sets for training and testing. Transfer learning based on a convolutional neural network (CNN) was applied in the background.

3 Model Evaluation : The platform provided immediate feedback on accuracy and class predictions, enabling adjustments to the balance and quality of the dataset.

4 Export and Deployment : Once the model achieved satisfactory accuracy, it was exported in TensorFlow Lite format, suitable for integration with the Raspberry Pi 4's camera module.

This classification included a balanced and structured dataset, enabling the AI system to distinguish between different defect types. The structured dataset was subsequently manually updated, with each image labeled according to its defect type, forming the basis for model training and evaluation.

V.3 AI Methods for Silo Inspection :

Artificial intelligence (AI) methods have become increasingly effective in automating wheat silo inspection. These methods can be broadly divided into traditional image processing techniques and machine learning/deep learning methods. Image processing provides rule-based detection based on visual features. This section details the basic AI methodologies used for automated defect detection and analysis in CPUs.

V.3.1 Image Processing and Enhancement :

Image processing is a method of performing operations on images in order to enhance them, extract meaningful information, or prepare them for further analysis. It involves techniques for improving image quality, restoring corrupted data, detecting features, compressing image files, and enabling interpretation by either humans or machines. The field combines concepts from mathematics, com- puter science, and engineering, and it serves as the foundation for applications in areas such as medical imaging, remote sensing, machine vision, and artificial intelligence.[23]

Digital image processing involves several basic steps to transform and analyze images. These steps include :

Image Acquisition : The first stage of the image processing process involves capturing images using a camera or scanner.

Image Enhancement : This procedure aims to improve the visual appearance of the image by reducing noise, adjusting contrast, and making geometric cor- rections.

Image restoration : This step aims to improve image quality by removing or reducing degradations, often based on a mathematical or probabilistic model of the degradation process.

Color image processing : This step aims to adjust color tones, saturation, and brightness.

Waveforms : Aimed at representing images at high resolution, which can be useful in image compression and analysis.

Compression : The compression process involves reducing the size of an image without compromising image quality, which facilitates its transfer and storage.

Morphological processing : This process extracts components useful for re- presenting and describing shape.

Segmentation : Image Segmentation is the process of assigning alabel to every pixel in an image. Is a sub field o fArtificial intelligence and computer vision. It istypically used to locate objects and boundaries in images. [24]

Object recognition : This aims to locate objects in images, which is important in computer vision.

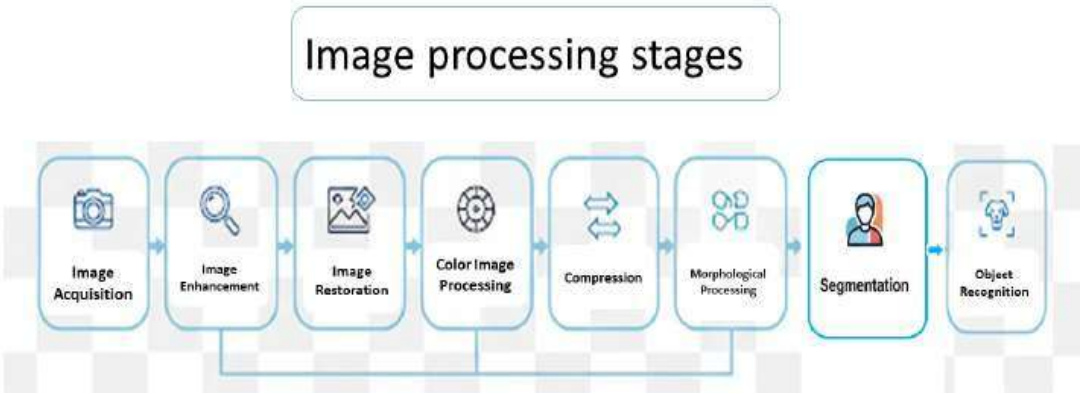

FIGURE V.2 – Image processing stages

V.3.2 Machine Learning :

Machine learning is an application of artificial intelligence (AI) that provides systems the ability to automatically learn and improve from experience without being explicitly programmed. It is a sub-area within the Artificial Intelligence domain. Machine learning focuses on the development of computer programs that can access data and use it learn for themselves. Thus when it encounters data it evaluates it to see if it fits a pattern and then takes action as prescribed by the pattern. If it does not fit a pattern then it takes predefined actions.[25]

V.3.3 Machine Learning Models :

Machine learning (ML) models represent the first generation of AI techniques applied to silo inspection before the widespread use of deep learning. These models rely on hand-crafted features extracted from images, such as color schemes, texture descriptors, or edge properties. Once the features are extracted, they are fed into traditional classifiers for defect detection and classification.

Several machine learning models have been widely applied to defect detection and classification :

Support Vector Machines (SVMs) : Effective in binary and multiclass classification problems. SVMs are particularly useful in distinguishing between defective and non-defective surfaces (e.g., cracked and uncracked) when feature vectors are accurately defined.

Random Forests (RF) :

A clustering method based on multiple decision trees. This method is robust to noisy datasets and can handle multiple classes, making it suitable for detecting corrosion, cracks, and biological damage.

K-Nearest Neighbors (k-NN) :

A distance-based algorithm that classifies new samples based on their similarity to previously classified images. Although easy to implement, its computational complexity increases with the size of the dataset.

Limitations :

Feature dependence : Performance is highly dependent on the quality of manually extracted features.

Limited generalization : Difficulty handling complex or overlapping anomalies under varying environmental conditions.

Lower accuracy : Generally less robust than deep learning models for large-scale real-world screening tasks.

V.4 Integration with Teachable Machine :

Teachable Machine, developed by Google, is an online platform that simplifies training machine learning models without the need for advanced programming knowledge. It allows users to upload labeled images for different defect classes and automatically generates classification models.

Integrating Teachable Machine into silo inspection offers several advantages :

Easy-to-use interface : Enables non-experts, such as field engineers, to quickly build and test models.

Rapid prototyping : Models can be trained and exported in various formats (TensorFlow, Keras, TensorFlow Lite, or ONNX) for deployment on various platforms, including the Raspberry Pi.

Custom dataset training : Supports training using images collected directly from silo inspections or from curated datasets (web sources, field images).

Cross-platform deployment : Facilitates instant inference on mobile devices, web browsers, or embedded systems.

The images were divided into five categories: rust ,vents,cracks, insects, and rodents. Here are some of the images we'll be working with:

FIGURE V.3 – cracks

FIGURE V.4 – Rust

FIGURE V.5 – Vents

FIGURE V.6 – insects

FIGURE V.7 – Rodents

Workflow Steps :

Open the Teachable Machine website, click Get Started, then select Image Project, then Standard Image Model.

Data Upload : Images are classified into categories (e.g., cracks, rust, insects, rodents).

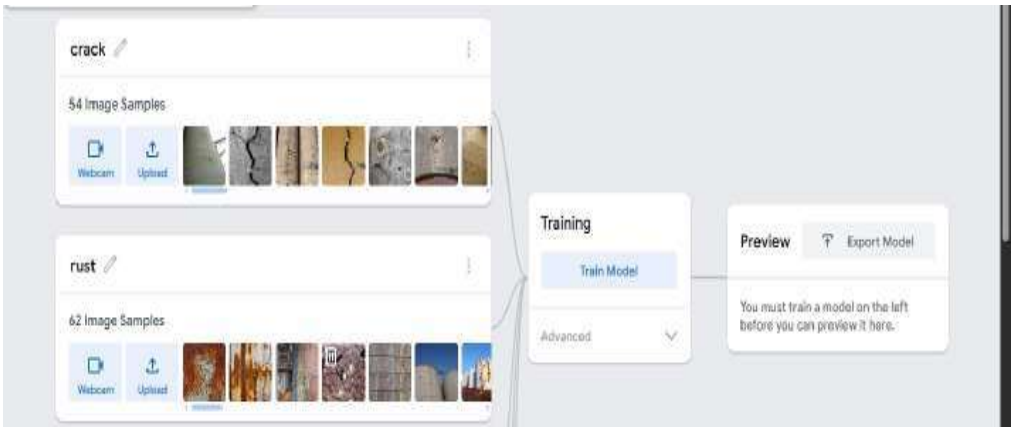

FIGURE V.3 – Upload Data

Model Training : Teachable Machine automatically trains a neural network using transfer learning techniques.

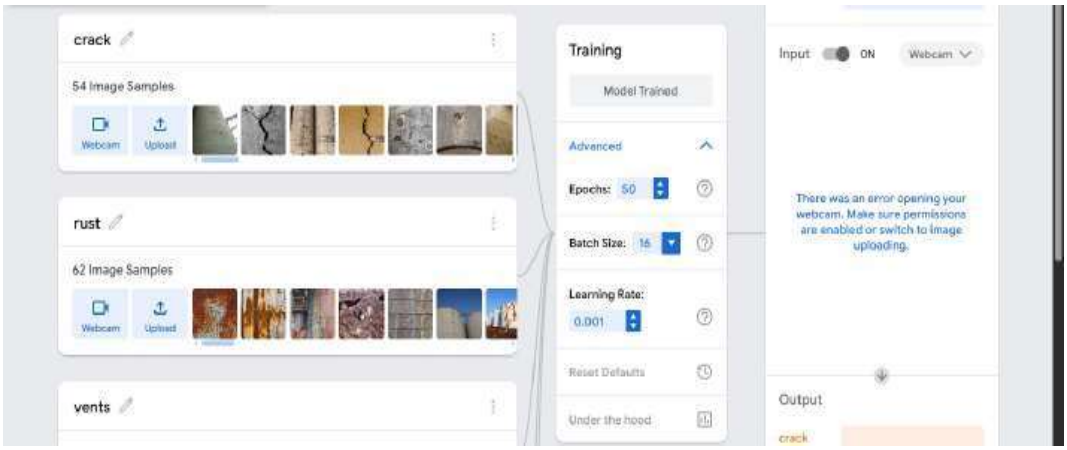

FIGURE V.4 – Model Training

Evaluation : The platform provides immediate feedback on the model's accuracy and confusion matrix.

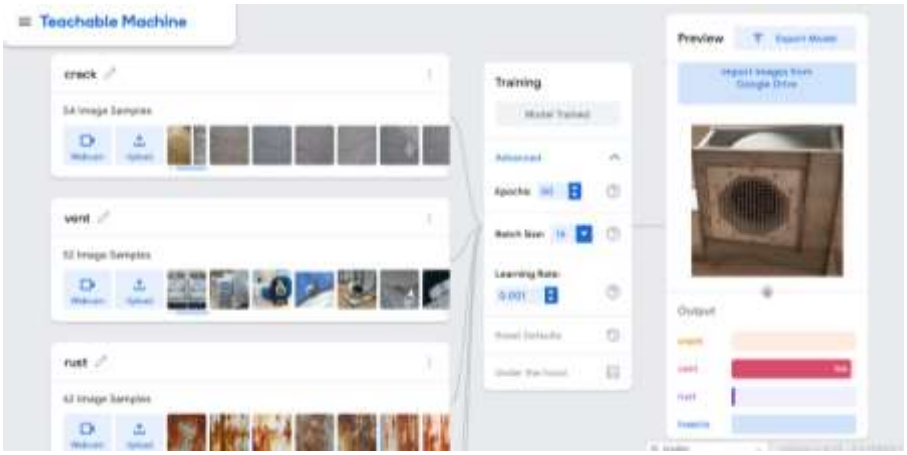

FIGURE V.5 – Evaluation

Export and Deployment : The trained model is exported and deployed to devices.

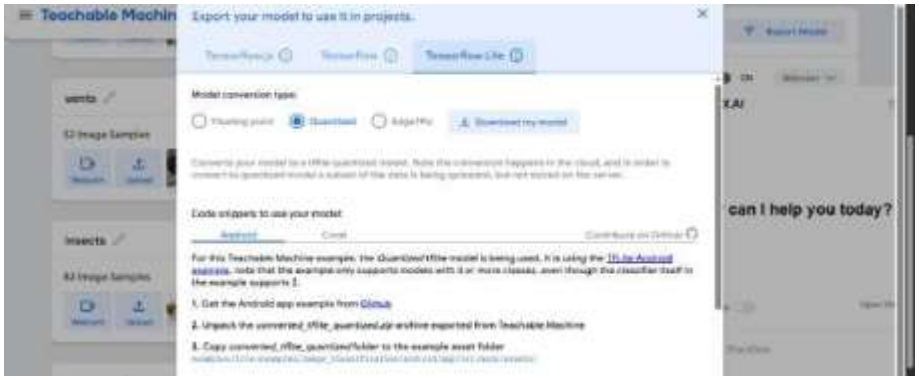

FIGURE V.6 – Export

V.5 Conclusion

In summary, this section highlighted the crucial role of data collection and AI-based methods in the inspection of wheat silos. By combining field training observations with online datasets, and leveraging image processing, machine learning, and Teachable Machine, it was possible to establish a preliminary framework for automated defect detection. These steps form the foundation for developing a smart and reliable inspection system that minimizes human risks while improving efficiency and accuracy.

Chapter VI :implementation and prototype

VI.1 Introduction

A quadcopter prototype is built upon the integration of multiple key sub-systems, combining electrical, mechanical, and software components in a cohesive manner to ensure flight stability and control. In this work, the proposed model is assembled using a widely adopted frame type (F450), which provides a stable base for component mounting. The flight controller used is the Mini Pix v1.2, which offers precise sensor integration and motor management. Power is sup- plied through a 3300mAh LiPo battery, while the Electronic Speed Controllers (ESCs) rated at 30A regulate the brushless motors, specifically the RS2205 mo- del with a 2300Kv rating. For remote communication, the system includes an FS-IA6B radio receiver, complemented by a GPS module for positioning and navigation, and a dedicated power module that ensures voltage regulation and monitoring. Together, these components form a functional platform suitable for experimentation in autonomous flight and intelligent inspection tasks.

VI.2

VI.3 Quadcopter Prototype and Main Components

VI.3.1 Frame : F450

The quadcopter frame is constructed from a composite material consisting of nylon reinforced with glass fiber, offering a balance between strength and light weight. It features a diagonal size of 50 cm, measured from the center of one mo- tor to the opposite motor, making it suitable for mid-sized UAV applications. The frame weighs approximately 280 grams when excluding motors and electro- nic components. Designed in a classic quad configuration, it includes four arms and supports propellers up to 23 cm in diameter. Additionally, the frame comes equipped with mounting holes and screws specifically intended for securing the flight controller at the center of the structure.

FIGURE VI.1 – Frame F450

VI.1.1 Flight Controller : Mini Pix v1.2

Processor and Sensors :

STM32F405VGT6 ARM microcontroller

InvenSense MPU6500

Compass QMC5883L Barometer LPS22HB Interfaces : 6x PWM outputs 1x

RC input (PWM/PPM, SBUS)

3 UARTS (flow-control on Telem 1 2, no flow-control on GPS port) external

I2C

2 x ADC for voltage and current sensor

1 x additional ADC for analog RSSI or analog airspeed SDIO

microSD card slot

micro USB connector

Includes buzzer / safety-switch, power module, I2C expansion board and TS100 GPS / mag combo depending on kit features

Size 39 x 39 x 12 mm

Weight 12 g without

wires

Role :"The brain of the aircraft" reads sensors, processes data, reads sensors, and controls motors to maintain balance and execute commands.[24]

FIGURE VI.2 – MiniPix

VI.1.2 LiPo Battery

Type : Lithium Polymer (LiPo)

Capacity : 3300mAh

Configuration : Typically 3S (three cells in series)

Weight : Approximately 250 grams

Role : Primary power source for the aircraft

FIGURE VI.3 – Lipo battery

VI.1.3 Electronic Speed Controller (ESC)

Maximum Continuous Current : 30 A

Supported Voltage : 2S to 4S Battery

Supports various control protocols : popular PWM (50 Hz)

Chapitre 2 Ports :

3 wires for motor output (marked A/B/C)

2 wires for battery (Power Input : + and -) via XT60 connector or similar

3 wires(VCC,GND, SIGNAL)for PWM signal to the Flight Controller Function : Controls the motor's rotation speed based on commands from the controller (Mini Pix).

FIGURE VI.4 – Electronic Speed Controller

VI.1.4 Motors : RacerStar RS2205

Model : RacerStar RS2205

Three-phase (Brushless) motor :

Stator Size : 22 mm (stator diameter) x 5 mm (stator height) Often designated as "2205".

KV : 2300 Kv i.e., the motor rotates at 2300 rpm at each volt Weight

(with screw and lock) : Approximately 2830 grams per motor

Overall Dimensions : Length 2526 mm, Outer Body Diameter 27.5 mm

Efficiency : 6.2 g/W

Function : Converts electrical energy into mechanical energy (propeller move- ment).

FIGURE VI.5 – Motors

VI.1.5 Radio Receiver : FS-iA6B

Type : FlySky FS-iA6B Protocol : AFHDS (Automatic Frequency Hopping Digital System)

Number of Channels : Up to 6 control channels (6 CH), including : Throttle Roll, Pitch Yaw, AUX1 (auxiliary channel that can be linked to functions such as autopathy or flight mode adjustment), AUX2 (additional auxiliary channel for other functions such as camera or LED activation)

Connectivity :

PWM output for each channel (6 wires), or PPM (Summation) output for one channel that carries all serial channels (if the Flight Controller provides a PPM input)

Supports Serial (i-Bus) communication to reduce wiring and transmit all chan- nels over a single wire.

Range : Up to approximately 1 km (in ideal conditions).

Telemetry : Supports sending some data (such as the battery level in the trans- mitter) if supported by peripherals

Function : Receives signals from the controller(PWM,PPM) and sends them to the Mini Pix controller.

FIGURE VI.6 – Radio Receiver

VI.1.6 GPS Module

It has a built-in GPS and compass. It is used for high-precision positioning.

It is compatible with controllers such as the Mini Pix.

It should be mounted away from electronic components to avoid magnetic interference.

Role : Precise geolocation and compass.

FIGURE VI.7 – GPS Module

VI.1.1 Power Module

Measures power consumption (current and voltage).

The Flight Controller is supplied with a constant voltage (e.g., 5V).

It has two outputs : one for XT60 power, and another for measuring the power supply.

Role :Powers the Mini Pix controller and Sends power consumption readings to the controller to monitor battery status.

FIGURE VI.8 – Power Module

VI.1.2 Transmitter : FS-i6X

Type : FlySky FS-i6X

LCD screen for displaying

settings. 6 to 10 channels

(updated).

2.4GHz frequency.

Role : Flight controller (sends commands to the FS-iA6B receiver).

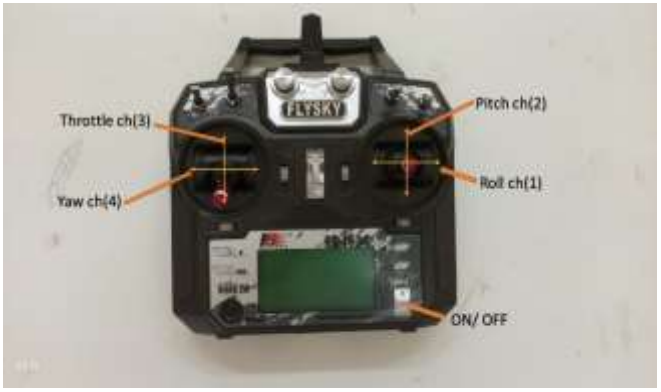

FIGURE VI.9 – Transmitter

VI.1.3 Propellers : Gemfan 1045

Type : Gemfan 1045

Length : 23.1 cm

Tilt Angle : 4.5 inches

Type : CW and CCW (clockwise and counterclockwise).

Role : Generates thrust to lift the aircraft. Height and pitch affect thrust and efficiency.

FIGURE VI.10 – Propellers

VI.1.4 Buzzer and Safety Switch

The buzzer issues alerts (such as low battery or signal loss

The Safety Switch is used to manually enable or disable flight for added safety.

FIGURE VI.11 – Buzzer and Safety Switch

VI.1.5 The MLX90614ESF-BCC sensor

This is a non-contact infrared thermometer developed by Melexis. It mea- sures the thermal radiation emitted by objects and provides high measurement accuracy over a wide temperature range. It supports the IšC communication protocol and can output via a PWM signal, making it suitable for robotics, me- dical systems, and Internet of Things (IoT) projects.

FIGURE VI.12 – Sensor MLX90614ESF-BCC

VI.1.6 The SG90 motor

The SG90 motor is a compact, lightweight servo motor that offers significant applications in robotics, educational engineering, and electronics projects. It uses a PWM (Pulse Width Modulation) signal to control the right angle, which can reach approximately 180 degrees.

FIGURE VI.13 – Servo motor

VI.1.7 Landing Gear

To provide adequate ground clearance for additional sensors, cameras, and a Raspberry Pi 4, 3D-printed landing legs were designed and manufactured. This design provides greater stability during takeoff and landing while maintaining light weight and compatibility with the F450 frame.

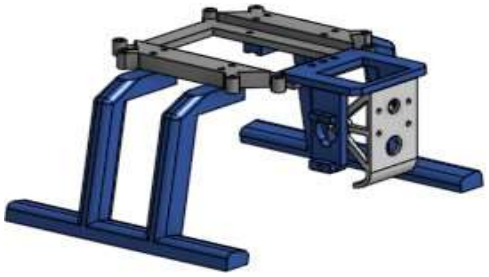

FIGURE VI.14 – 3D printed landing gear designed for the F450 frame.

VI.1.8 Raspberry Pi Camera Module 2 Wide

The Raspberry Pi Camera Module v2 NoIR is an official camera from the Raspberry Pi Foundation, equipped with an 8-megapixel Sony IMX219 sensor. It is capable of capturing high-quality still images and video recording at up to 1080p30, 720p60, and 640Œ480p90.

The NoIR (No Infrared filter) version does not include an infrared filter, which allows it to capture images in low-light conditions and to work with infrared illumination.[25].

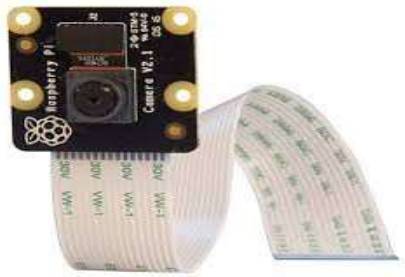

FIGURE VI.15 – raspberry pi camera module 2 noir

VI.1.9 System Connection Diagram

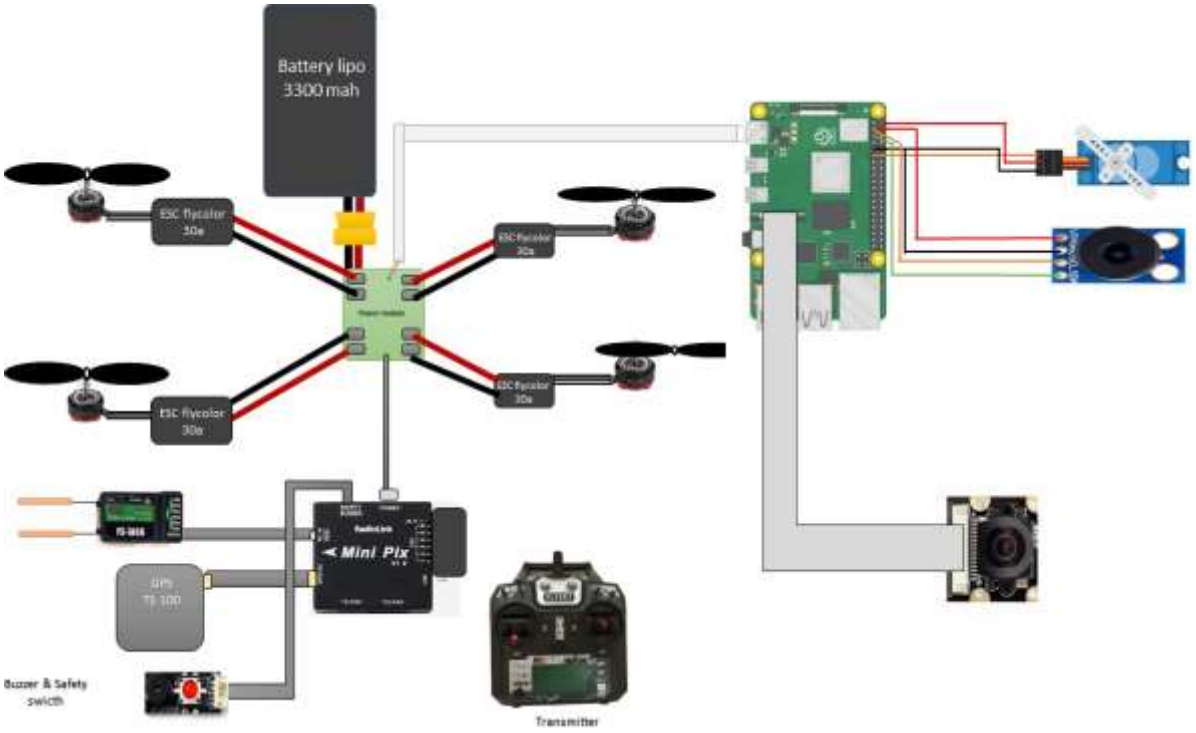

FIGURE VI.16 – System Connection Diagram

VI.2 Mission Planner Software

VI.2.1 Roles and Functions

Mission Planner is a ground control station (GCS) software for setting up and managing ArduPilot/APM drones, and is the primary choice for those using flight controllers such as the Pixhawk or Mini Pix.

VI.2.2 Firmware Setup and Sensor Calibration

Allows the user to install or update the ArduCopter, ArduPlane, or other version of the flight controller.

The user selects the type of aircraft (Quadcopter, Hexacopter, Fixed Wing, etc.) and then downloads the appropriate software.

Sensor Calibration : Gyro, Accelerometer, Compass, and ESC Calibration.

VI.2.3 Waypoint Planning and GPS Use

Mission Planning : Waypoints can be plotted directly on the built-in map interface (usually Google Maps or OpenStreetMap). Specific actions can be ad- ded, such as taking a photo, changing altitude, or adjusting flight speed. Real- time battery level display.

GPS data reading : location, altitude, ground speed, and orientation on the map. Graphs display sensor values such as acceleration, roll/pitch/yaw. Advan- ced Parameter Tuning

.**Parameter Tuning and Telemetry**

Allows you to adjust hundreds of parameters related to PID stability control, speed limits, camera settings, and more. A specific setting can be saved and later applied to other aircraft. Graphs display sensor values, RC inputs, and more, helping diagnose problems and improve performance.

VI.3 Connection between minipix and mission planes :

Establishing a connection between the Mini Pix v1.2 flight controller and the Mission Planner software is the first and essential step for configuration, calibration, and mission planning. It allows for firmware uploading, sensor ca- libration, and calibration of the electronic speed controllers, radio transmitter, and battery.

VI.4 Connecting Mini Pix to Mission Planner

VI.4.1 Installation and Initial Connection

The Mission Planner software is installed from the official website. https: //ardupilot.org/planner/docs/mission-planner-installation.html

The Mission Planner program is installed from the official website. After ins- tallation, we connect it to a USB port and then launch the Mission Planner program. A map and gyroscope interface will appear. First, we connect a micro USB Type A cable to the MiniPix and another to the computer.

At the top right, we see the COM port selected for the computer’s connection and the Serial Communications selection, which is 115200.

Then, we click Connect, which will establish a connection between the computer and the MiniPix.

The Mission Planner program is installed from the official website.

After installation, we connect it to the USB port and then launch the Mission Planner program.

A map and gyroscope interface will appear.

Once we have installed the station on our computer, we connect the autopilot using a USB cable as shown. We use a direct USB port on our computer (not a hub USB).

Then, we click Setup to move to the next step.

FIGURE VI.17 – Mission Planner

VI.4.2 Firmware Uploading

In the second step, we'll discuss installing the firmware. We'll click the "Dis- connect" button in the upper-right corner of the screen. A screen will appear as shown in the second image. We will click the third icon (the helicopter). The firmware will be downloaded and sent to Minipix.

FIGURE VI.18 – Installing the firmware 1

FIGURE VI.19 – Installing the firmware 2

Then we will move to mandatory hardware and then to frame type, where we will see several forms, including the one we chose.

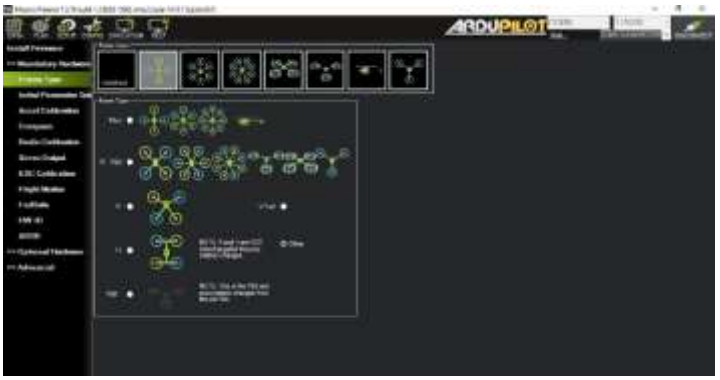

FIGURE VI.20 – Frame type

Then, in mandatory hardware, click on accel calibration. In this option, we will work on calibration, where the quadcopter is placed on a flat surface, and then we are asked to place it on the right, left, front, and back sides.

FIGURE VI.21 – Accel calibration

Then, in mandatory hardware, go to compass. In this option, we will work on calibrating the compass, which is the compass that moves the drone in all direc- tions. It is a sensor used to measure direction and determine the direction, and enables the pilot or the automated system to know in which direction the drone is heading (north, south, east, west).

FIGURE VI.22 – Compass

Then, in mandatory hardware, go to radio calibration. In this option, we will work on calibrating the radio transmitted from the F-Si6X, which are the values of the channel signals, such as the stick roll throttle pitch yaw. From this, you will see the final values for each stick : 1000-2000. At the beging, each stick will be in its initial state.

FIGURE VI.23 – Radio calibration

Next, in mandatory hardware, go to calibration ESC. In this option, we will calibrate the electronic speed control unit for the motors used in the drone. This is a process in which the ESC is informed of the range of signals coming from the control unit so that it can correctly interpret the acceleration commands. This step is necessary to ensure that all motors operate with the same power.

FIGURE VI.24 – Calibration ESC

After that, in mandatory hardware, we will select the calibration esc. In this op- tion, we will work on determining the flight mode, and each mode has a different level of control. These modes include : Stabilize, AltHold, Loiter, RTL (Return To Launch), and Auto Acro Land.

FIGURE VI.25 – Flight mode

Flight Mode is the phase in which the control method of the quadcopter during flight is determined, i.e. how the aircraft behaves in response to commands from a transmitter.

FIGURE VI.26 – Failsafe

Failsafe is a protection system that automatically makes the drone behave in a specific way (such as landing or returning to the take-off point) when a sudden problem occurs, to protect it from falling or getting lost.

FIGURE VI.27 – motor test

Here, the motors will be tested to ensure the correct orientations (CW or CCW rotation). The motors are securely mounted and do not vibrate.

VI.1 Raspberry Pi Integration

Raspberry Pi is a series of small single-board computers developed in the United Kingdom by the Raspberry Pi Foundation in collaboration with Broad- com. To commercialize the product and support its growing demand, the Foun- dation established a commercial entity, Raspberry Pi Holdings, a public company that trades on the London Stock Exchange. The Raspberry Pi was originally created to help teach computer science in schools, but gained popularity for many other uses due to its low cost, compact size, and flexibility. It is now used in areas such as industrial automation, robotics, home automation, IoT devices, and hobbyist projects.[23].

VI.1.1 Hardware Features of Raspberry Pi 4

The Raspberry Pi 4 features significant improvements over previous versions, making it suitable for advanced tasks such as computer vision. Its most notable components include :

Processor : 1.5GHz quad-core ARM Cortex-A72, providing high performance for image and data processing.

RAM : Multiple options (2GB, 4GB, or 8GB), enabling efficient running of

complex algorithms.

Input/Output Ports : Includes USB 3.0/2.0 ports, two micro-HDMI ports, and an Ethernet port, expanding connectivity possibilities.

GPIO Ports : Used to control external devices such as motors or sensors. **Camera Ports (CSI) :** For connecting regular or thermal Raspberry Pi came- ras.

These components enable efficient integration with advanced drone and sensor systems.

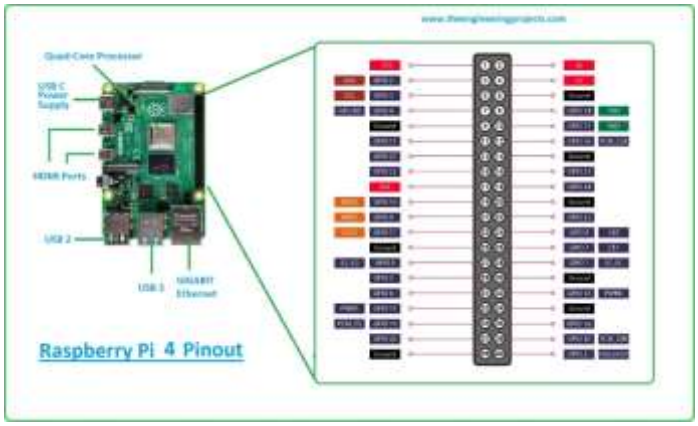

FIGURE VI.28 – Raspberry Pi 4

VI.1.2 Using Raspberry Pi in Computer Vision

In this project, a Raspberry Pi 4 is used to run computer vision algorithms, enabling the smart drone to analyze images captured during flight. Both a regular (RGB) camera and image processing are connected to the device. For example, cracks in the silo structure or heat leaks are detected using edge detection and deep learning techniques. This local processing on the Raspberry Pi reduces the need to transfer raw data, providing rapid responses and contributing to real-time smart decision-making.

VI.1.3 The Role of the Raspberry Pi in Smart Silo Inspection

The Raspberry Pi 4 plays a pivotal role in implementing smart silo inspec- tion tasks. It acts as the "brain" responsible for collecting and analyzing data from thermal and regular cameras, and connecting the results to the drone's guidance system. Images are analyzed to detect indicators that may indicate leaks, cracks in the walls, or structural or environmental issues. The Raspberry Pi is also used to record images

and data, converting them into technical reports or sending them to a cloud server when connectivity is available. This ability to process and interact on-site makes the system more independent and effective in inspection.

VI.1 Prototype

The main components of the quadcopter :

frame F450

Controller : Mini pix

v1.2 Propellers :

Gemfan 1045

Electronic speed controllers 30 A

Motor BLDC RS2205 2300 kv

Receiver FS-

iA6B GPS TS

100

Battery lipo 3300 mah

Raspberry pi 4

Raspberry pi camera module v2 noir

temperature sensor Mlx90614 gy-906 bcc

Servo motor sg90

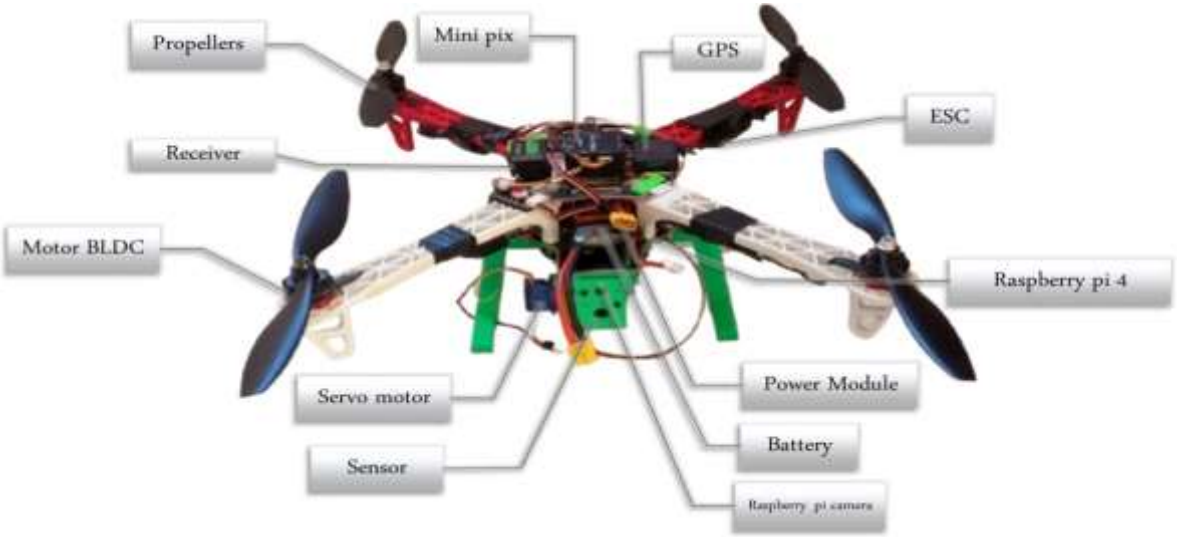

FIGURE VI.29 – Protoype

FIGURE 1 : Photo prototype 1

FIGURE 1 : Photo prototype 2

FIGURE 1 : Photo prototype 3

VI.2 Conclusion

By integrating smart drone technology with normal vision, it has become possible to inspect wheat silos. During this project, a drone was designed with a Mini Pix v1.2 flight controller, a GPS module, electronic control units (ESCs), and a 3300 mAh lithium polymer battery. The drone was programmed and calibrated. In addition, by integrating a Raspberry Pi 4, images will be uploaded and processed by training a model to classify images such as cracks, rust, stairs, and vents.

General conclusion and future directions

General conclusion and future directions

This master's thesis has successfully demonstrated the viability and significant advantages of an integrated smart drone system for the automated inspection of wheat silos. The research journey began with establishing a rigorous mathematical foundation, deriving a comprehensive nonlinear dynamic model of the quadcopter that accurately captures its complex flight behavior. This model served as the essential bedrock for control system design, where a comparative analysis between a classical PID controller and an advanced Sliding Mode Control (SMC) strategy was conducted. The results unequivocally confirmed the superior robustness and precision of the SMC in trajectory tracking and disturbance rejection, making it the recommended control paradigm for real-world applications characterized by uncertainties and external perturbations.

Beyond stable flight, the project's core innovation lies in its intelligent inspection capability. By leveraging artificial intelligence, specifically a convolutional neural network trained on a custom-curated dataset, the system transcends mere data collection to achieve automated defect diagnosis. The developed prototype, integrating a MiniPix flight controller, dual-vision sensors, and a Raspberry Pi for onboard processing, stands as a tangible proof-of-concept. It validates a complete workflow—from autonomous navigation and real-time image acquisition to AI-powered analysis of structural and thermal anomalies such as cracks, rust, and pest infestations.

In conclusion, this work effectively bridges the critical gap between theoretical control engineering and practical industrial application. It presents a holistic solution that not only addresses the limitations of traditional, hazardous, and costly manual inspections but also paves the way for a new standard in predictive maintenance and asset management. By enhancing operational safety, improving inspection frequency and accuracy, and reducing human intervention, this smart drone technology marks a substantial step forward in the modernization of agricultural and industrial infrastructure monitoring.

Future work will focus on enhancing the system's capabilities through advanced sensor fusion (like LiDAR), more powerful onboard AI for real-time defect segmentation, and fully autonomous navigation using SLAM technology. The deployment of cooperative drone swarms could drastically reduce inspection times, while integrating predictive analytics would enable forecasting defect progression. Further hardware optimization for endurance and specialized payloads, alongside ensuring robust regulatory compliance and data security, will be crucial for widespread industrial adoption.

Reference

References

[1] Vincent Ambrosia, Foreword to the Special Issue on Unmanned Airborne Vehicle (UAV) Sensing Systems for Earth Observations,

[2] T-drones, Quadcopter Drones,

[3] WikipediaElectronic speed control, Electronics, vol. 13, no. 5, pp. 820, 2024.

[4] Daniel sanfelice modalai Flying drones : motor and problles,x

[5] drone lab, Quadcopter Flight Controllers : The Process Behind Every Quad-copter,

[6] T-dronesTransmitter and receiver,Quadcopter Drones : A Comprehensive Beginners Guide

[7] umiles Camera and Video,What are the parts of a Drone ? Full list

[8] Quadgeek, GPS Module,

[9] Gopal Dutta ,Purba Goswami , Security Drones : An In-Depth Guide .

[10] Online Drone courses, Security Drones : An In-Depth Guide .

[11] CCS Group LLC, The Drone Inspection Process : From Desire to Data Deliverables .

[12] C. Van Tilburg, First Report of Using Portable Unmanned Aircraft Systems (Drones) for Search and Rescue .

[13] Tejinder Singh Lakhwani, Yerasani Sinjana, Anuj Pal Kapoor, Queuing theory for efficient drone dispatch in healthcare logistics : An empirical ana- lysis of system performance

[14] Dukeforest, How Drones are Transforming Research in the Duke Forest and Beyond .

[15] Suresh, H. (2021). Quadcopter Control : Modelling, Simulation and Imple-mentation.

Reference

[16] H. Bolandi, M. Rezaei, R. Mohsenipour, H. Nemati, and S. M. Smailzadeh, Attitude Control of a Quadrotor with Optimized PID Controller, Intelligent Control and Automation, vol. 4, no. 4, pp. 335–342, 2013.

[17] K. J. Åström and R. M. Murray, Feedback Systems : An Introduction for Scientists and Engineers, Draft version v2.4a, 2006.

[18] M. Hammou, Modélisation, Commande et Simulation dun Quadrirotor, Mémoire de Master, Université de Ghardaïa, 2021.

[19] Kumar, R ,Research Methodology : A Step-by-Step Guide for Beginners (5th ed.). SAGE Publications.

[20] Image Processing,Image Processing, Gonzalez, R. C., Woods, R. E. (2018).

[21] Digital Image Processing (4th Edition). Pearson

[22] Raksha S Kale,Dr. Surabhi Thorat (2021) Image Segmentation Techniques with Machine Learning, International Journal of Scientific Research in Com- puter Science

[23] Sunit Chaudhury. 2018 , What is Machine Learning, Types of Machine Learning and Programming Languages used in Machine Learning

[24] wikipedia,raspberry pi,

[25] RadioLink MiniPix ,Specifications Minipix v1.2,

[26] Raspberry Pi Foundation , Raspberry Pi Camera Module v2 NoIR.

الجمهورية الجزائرية الديمقراطية الشعبية

وزارة التعليم العالي والبحث العلمي

Université de Ghardaïa
Faculté des Sciences
et de la technologie

جامعة غرداية
كلية العلوم والتكنولوجيا
قسم :الآلية والكهروميكانيك

شعبة :... الآلية .....

تخصص:.... الآلية والكهروميكانيك

غرداية في :.2025/11/04

شهادة ترخيص بالتصحيح والايداع:

انا الاستاذ(ة)..... بكار بلقاسم .....

بصفتي المشرف المسؤول عن تصحيح مذكرة تخرج (ليسانس/ماستر/دكتورا) المعنونة بـ:

Smart Drone Technology for comprehensive Wheat Silo Inspection Integrating Normal and Thermal Vision

من انجاز الطالب (الطلبة):

جبلي محمد نور الدين

.....

التي نوقشت بتاريخ : 2025/10/22

اشهد ان الطالب/الطلبة قد قام /قاموا بالتعديلات والتصحيحات المطلوبة من طرف لجنة المناقشة وقد تم التحقق من ذلك من طرفنا

وقد استوفت جميع الشروط المطلوبة.

جامعة غرداية
بكار بلقاسم
مكلف بالدراسات القسم الآلية والكهروميكانيك
كلية العلوم و التكنولوجيا

مصادقة رئيس القسم

إمضاء المسؤول عن التصحيح